Applied Energy 316 (2022) 119118

Contents lists available at ScienceDirect

Applied Energy

journal homepage: www.elsevier.com/locate/apenergy

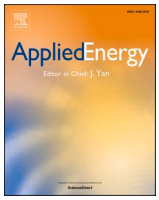

Techno-economic analysis of the transition towards the large-scale hybrid wind-tidal supported coastal zero-energy communities

Ming Li [a], Sunliang Cao [a,c,d,*], Xiaolin Zhu [b,c], Yang Xu [b,c]

[a] Renewable Energy Research Group (RERG), Department of Building Environment and Energy Engineering, Faculty of Construction and Environment, The Hong Kong Polytechnic University, Kowloon, Hong Kong SAR
[b] Department of Land Surveying and Geo-Informatics, The Hong Kong Polytechnic University, Kowloon, Hong Kong SAR
[c] Research Institute for Sustainable Urban Development (RISUD), The Hong Kong Polytechnic University, Kowloon, Hong Kong SAR
[d] Research Institute for Smart Energy (RISE), The Hong Kong Polytechnic University, Kowloon, Hong Kong SAR

HIGHLIGHTS

- Realization of coastal zero-energy communities by hybrid wind-tidal energy systems.
- Comparison between wind-based and tidal-based renewable energy generations.
- Impact of renewable mixing of offshore wind and tidal on the system performances.
- Solutions of energy matching enhancement for large-scale hybrid wind-tidal systems.
- Techno-economic feasibility analysis of the hybrid offshore wind-tidal system.

ARTICLE INFO

Keywords:
Coastal zero-energy community
Tidal stream energy
Offshore wind energy
Hybrid renewable energy system
Community-scale electricity storage

ABSTRACT

In the current academic fields of zero-energy community, there is still limited knowledge on the integration of a coastal community with hybrid ocean-related energy systems. This study investigates the feasibility of a coastal community to reach zero-energy with the support of a hybrid offshore wind and tidal stream energy generation system, as well as an ocean and solar thermal energy supported district cooling and heating system. TRNSYS simulation was performed to demonstrate a proposed community that comprises 8 high-rise residential buildings and 2 mid-rise office buildings with a 9.86 MW community peak power demand. This study considered 21 hybrid renewable energy cases and investigated their performance in 2 scenarios – scenario 1 without battery and scenario 2 with battery. The system performance is assessed from the technical, economic, and emission perspectives by analysing the system load matching, net present value, discounted payback period, and equivalent CO_2 emission. In scenario 1, the hybrid renewable energy case 5 with 6 offshore wind turbines (12 MW) and 117 tidal stream converters (29.25 MW) has the best annual load matching (56.68% "onsite energy matching" and 57.84% "onsite energy fraction") mainly due to their complementary generation pattern during specific periods. In scenario 2, the community-scale electricity storage significantly increases the system technical performance by raising the "onsite energy matching" and "onsite energy fraction" of case 5 to 75.25% and 74.75%, respectively. In addition, the techno-economic analysis reveals the market competitiveness of the 21 RE cases and demonstrates the significant economic impact of the FiT policy. The comparison between scenario 1 and scenario 2 indicates that the community-scale battery diminishes the operation-cycle profits but reduces the equivalent CO_2 emission. Furthermore, with the current price settings, tidal stream energy generation is considered less profitable than offshore wind energy generation. This study could provide important insights into the development of coastal zero-energy communities with hybrid offshore wind and tidal stream energy generation at other locations worldwide, especially densely populated coastal cities.

* Corresponding author at: Renewable Energy Research Group (RERG), Department of Building Environment and Energy Engineering, Faculty of Construction and Environment, The Hong Kong Polytechnic University, Kowloon, Hong Kong SAR.
E-mail addresses: sunliang.cao@polyu.edu.hk, caosunliang@msn.com (S. Cao).

https://doi.org/10.1016/j.apenergy.2022.119118
Received 21 November 2021; Received in revised form 30 January 2022; Accepted 11 April 2022
Available online 19 April 2022

1. Introduction

1.1. Background

Nomenclature

AHU	air handling unit
$B_{FiT,n}$	annual FiT subsidy in the year n
$B_{saving,n}$	the annual saving from operating the community energy system during the year n
C_{CAPEX}	the capital investment cost
$C_{CAPEX,ref}$	the capital investment cost of the reference case
$C_{O\&M,n}$	annual operation and maintenance cost in the year n
$C_{O\&M,n,ref}$	annual operation and maintenance cost of the reference case in the year n
C_{tariff}	electricity tariff
$CAPEX$	capital expenditure/investment cost
$CAPEX_{OWT}$	capital installed cost of OWT per MW
$CAPEX_{TSC}$	capital installed cost of TSC per MW
CEF_{eg}	The equivalent CO_2 emission factor of the electric grid (kg CO_2e /kWh)
CO_2e	annual equivalent CO_2 emission
COP	coefficient of performance
DHW	domestic hot water
DPP_{rel}	discounted payback period relative to the reference case
$E_{export,n}$	the annual RE exported to the grid in the year n
$E_{generation,n}$	annual RE generation in the year n
$E_{import,n}$	annual imported energy in the year n
$E_{import,n,ref}$	annual imported energy of the reference case in the year n
$E(t)$	instantaneous power exported to the grid (kW)
FiT	Fit-in Tariff
$FSOC$	fraction state of charge
$G(t)$	instantaneous RE generation (kW)
i	interest rate
$I(t)$	instantaneous power imported from the grid (kW)
$L(t)$	instantaneous community load (kW)
$LCOE$	levelized cost of energy
NPV_{rel}	net present value relative to the reference case
$nZEC$	nearly Zero-Energy Community
OEF	onsite energy fraction
OEM	onsite energy matching
OWT	offshore wind turbine
$P(t)$	instantaneous power production (kW)
PV	photovoltaic
RE	renewable energy
$U(t)$	instantaneous tidal stream speed (m/s)
ZEC	zero-energy community

In recent decades, climate change has become a widely discussed topic as global warming and abnormal weather phenomenon become increasingly noticeable. With the urgency in mitigating climate change, a legally binding international treaty – the Paris Agreement, was adopted by 196 parties of the United Nations in 2015. The Paris Agreement aims at limiting global warming well below 2 °C compared to pre-industrial levels and requires the 196 parties to reach the peak of greenhouse gas emission as soon as possible [1]. With the ambitious targets of reducing carbon emission, nations have been striving to increase the penetration of renewable energy (RE) in their energy consumption. According to the International Energy Agency [2], the share of RE in the global electricity market had reached 29% in 2020 and will further expand by more than 8% in 2021, contributing more than 8,300 TWh electricity. Moreover, according to International Renewable Energy Agency [3], the global RE capacity in 2020 had reached 2,802 GW, accounting for 36.5% of the global electricity capacity and doubling the global RE capacity in 2011. While international RE development has been showing promising progress in the last decade, the development of larger-scale inland solar and wind energy systems in densely populated coastal cities will be largely restricted by the precious land resources. Exploiting an open field solely for the installation of solar and wind energy systems is hardly considered feasible. However, with their geographical advantage of being close to the sea, the development of ocean-related RE, such as offshore wind energy and tidal stream energy, is of great potential.

While it is commonly believed that RE can contribute to the reduction of carbon emission, problems such as the intermittency of RE will pose increasing challenges to the stability of the main electric grid. One of the solutions to reduce the influence of RE systems on the existing grid could be consuming the RE generation locally before the interaction with the main grid. In addition, energy storage can be coupled to improve the load matching, and subsequently, increase the local RE utilization while minimising the grid interaction and the RE curtailment. When the RE generation is sufficient to cover the energy consumption of a cluster of buildings, a zero-energy community (ZEC) is formed. According to the National Renewable Energy Laboratory [4], a ZEC can be defined as "a community that has greatly reduced energy needs through efficiency gains such that the balance of energy for vehicles, thermal, and electrical energy within the community is met by renewable energy". In other words, a ZEC can be achieved by firstly reducing the energy consumption, and secondly coving the energy consumption by RE generation. To evaluate if a ZEC is achieved, a community system boundary should be defined. In this study, the system boundary is set at the interface with the electric grid, which is naturally left outside the boundary as it falls on the scope of public utility. In addition, vehicles are excluded from the community energy system. Thereafter, the duration for evaluating the net energy balance should be specified. In this study, the criteria of achieving zero-energy are determined based on the overall annual energy balance, meaning that the community is considered a ZEC if the annual RE generation is sufficient to cover the annual community energy demand, including any energy loss induced. Due to the non-dispatchable attributes of most RE generation, the instantaneous system load matching can hardly be controlled at 100%. Therefore, there could be excessive RE generation exported to the grid and RE generation deficit that has to be compensated by importing electricity from the grid at any moment throughout the year. In this case, although grid interaction is unavoidable, the community is still considered a ZEC if the amounts of exported RE exceed the amounts of imported grid electricity, because the net energy balance at the system boundary fulfils the criteria of a ZEC.

1.2. Literature review

The availability of tidal stream energy sources has been studied in many places around the world. Gao et al. [5] assessed the potential of tidal stream energy generation around the Hulu Island of Zhoushan, China, where the maximum tidal stream speed was found greater than 1.7 m/s and the distributed depth-average tidal stream speeds are between 0.6 and 1.0 m/s. The average power density reaches 1.81 kW/m^2 at one of the selected sites. Orhan and Mayerle [6] studied the tidal stream energy potential at the Strait of Larantuka, Indonesia. It was estimated that the tidal stream speed can reach up to 3–4 m/s, and the average tidal stream power density is 10 kW/m^2. Marta-Almeida et al.

[7] observed a 1,300 W/m^2 tidal stream power density at the surface layer of the Bay of All Saints, Brazil. At the same location, the tidal stream speed is higher than 1 m/s during 30% of the time.

The feasibility of tidal stream energy generation has been discussed from the perspective of the technology and the techno-economic performance. Roberts et al. [8] reviewed the prevalent nearshore tidal energy conversion technologies, including tidal turbine, oscillating hydrofoil, tidal kite, and tidal range. It was found that cross-flow tidal turbine is the most suitable technology for nearshore applications because of the high power density and the less stringent requirement on the water depth. Lewis et al. [9] developed a standardised tidal-stream power curve based on 14 commercially available horizontal axis tidal stream turbines. It was found that the general cut-in speed is around 30% of the rated speed. In addition, it was stated that the most optimal rate speed of the turbine should be 50% or greater than 87% of the maximum tidal current speed at the site. From the economic perspective, Gross et al. [10] developed a novel cost reduction methodology that can be used to optimise the number of tidal stream converters, and subsequently, the spatial distribution of the array. To further optimise the system techno-economic performance, hybrid tidal energy generation has also received some attention in the academic. For example, Soudan [11] discussed the possibility of utilizing wave, tidal stream, and tidal range energy to support a coastal community. It argued that tidal stream energy generation is the appropriate and cost-effective choice due to the consistent energy generation. Pearre, Adye, and Swan [12] studied hybrid wind, solar, and tidal stream energy generation by coordinating the proportion of the three energy generation capacity. It was found that 61% wind, 27% solar, and 12% tidal stream energy generation is the optimal combination when considering the energy generation, power output, ramp rate, etc. Furthermore, Lande-Sudall, Stallard, and Stansby [13] studied the possibility of co-locating offshore wind turbines (OWTs) at a tidal stream energy generation site to reduce the cost of electricity. The case study at the MeyGen site in Pentland Firth concluded that the levelized capital cost of energy and the cost of energy will both decrease with the increasing co-located offshore wind energy capacity.

Compared to tidal stream energy generation, the potential and techno-economic feasibility of large-scale offshore wind developments have been more comprehensively studied worldwide. For example, Wen, Kamranzad, and Lin [14] investigated the potential of offshore wind energy generation in the south and southeast coasts of China using the 55-year data. The annual energy generation at 19 selected sites was estimated with 12 OWT models. Specifically, the annual wind energy generation reaches 35.36 MWh with a 7 MW OWT along the coast of Hong Kong. Gao et al. [15] proposed a multi-population genetic algorithm for optimizing the offshore wind farm layout. A case study was conducted in Hong Kong with forty 5 MW OWTs arranged in the optimized layout in a 62.86 km^2 area. The annual energy generation reaches 7.25x10^8 kWh, and the LCOE is 0.19 USD/kWh. In Europe, Caglayan et al. [16] found that 31.5% of the marine areas are suitable for offshore wind energy generation. With the cost-optimal offshore wind turbine selection, the overall offshore wind capacity and energy generation across Europe could reach nearly 8.6 TW and 40.0 PWh at the levelized cost of energy (LCOE) around 7 Euro-Cent/kWh by 2050. In the Northern Adriatic Sea, Schweizer et al. [17] estimated that a 3.6 MW offshore wind turbine could generate 7.88 GWh energy each year with a 25% capacity factor. Furthermore, a 216 MW offshore wind farm could achieve a net present value (NPV) of 17.11 million Euro with an 8.12% internal rate of return. Additional techno-economic studies has been conducted in Kuwait [18], Turkey [19,20], Chile [21], Philippines [22], India [23], etc.

In addition, several studies discussed the possible integration of offshore wind systems and energy storage to improve the overall techno-economic performance Liu et al. [24] developed an optimization model for assessing the techno-energy-economic performance of the offshore wind-pumped storage power system. The storage system performance was evaluated by the pumping state, the discharging state, and the state of charge. A case study was conducted in the south-eastern part of Liaoning Province. In addition to pump storage, Li and DeCarolis [25] examined the techno-economic performance of an offshore wind farm with compressed air storage. The optimised result indicated a LCOE around 0.3 USD/kWh when the capacity factor is higher than 90%. Simpson et al. [26] proposed the concept of co-locating liquid metal batteries at the substructure of an OWT. The study demonstrated that the co-located liquid metal batteries would increase the system values and argued that co-locating Li-ion batteries would also be beneficial as technologies improve in the future.

With the abundant RE resources, achieving zero energy becomes possible at the community scale. Fouad, Iskander, and Shihata [27] simulated a ZEC with 52 buildings in Egypt. The ZEC is supported by PV panels and wind turbines. Compared to a conventional community, the ZEC saves 57.6% of annual energy consumption and reduces 390 tons of equivalent CO_2 emission. Lopes et al. [28] studied the load matching of a cooperative ZEC, which is supported by PV generation. It was found that 46% of the annual community demand can be directly covered by 39% of the annual PV generation. Barone et al. [29] developed a dynamic simulation tool aiming to investigate the feasibility of a community to achieve zero energy. The case study in El Hierro revealed that the wind-powered pumped hydro-storage system could cover 85% of the community electricity demand, while the solar thermal collectors could provide 79% of thermal energy demand. Moreover, Jahangir, Shahsavari, and Rad [30] investigated the cost of deploying multiple hybrid RE systems to support a 3,000 household community in Iran. The case study indicated that the hybrid PV and wind turbine system with battery is the most cost-effective solution. Vindel, Berges, and Akinci [31] explored the possible approaches to reduce the grid interaction of a ZEC with 40 residential and non-residential buildings. Through an energy sharing and storage network, the annual grid interaction can be effectively reduced by 9.5%.

Furthermore, there are more and more studies in the field of ZEC discussing the integration of hydrogen storage and hydrogen vehicles. For example, Liu et al. [32] studied the techno-economic-environmental feasibility of a ZEC comprising a university campus, commercial offices, and high-rise residential buildings. In the case with a hybrid PV and wind energy generation system, stationary Li-ion batteries, and hydrogen vehicles, the ZEC achieves a 95.86% self-consumption ratio, a 66.62% load coverage ratio, and a 50.96% hydrogen system efficiency. Economically and environmentally, the ZEC increases the NPV by 96.17% and reduces the CO_2 emission by 71.23%. In addition, a hybrid electricity-hydrogen district sharing system integrated with rooftop PV systems, hydrogen vehicles, a hydrogen station, a microgrid, and hydrogen pipelines can be found in [33].

1.3. Scientific gaps and objectives

Based on the above literature review from the global scale, several scientific gaps regarding hybrid renewable energy generation and ZEC can be identified internationally:

(1) There is limited knowledge on hybrid offshore wind and tidal stream energy generation. Recent research involving hybrid RE generation mainly investigates the combination of solar PV and wind energy, while relatively less attention has been paid to the potential, benefit, and feasibility of hybrid offshore wind and tidal stream energy generation. Compared to other RE sources, tides are highly predictable and occur periodically [34], and thus, the tidal stream is able to provide a more consistent and stable energy generation throughout the year. Together with the land saving potential, the continuously decreasing cost, and the widespread applications of offshore wind energy generation, the techno-economic feasibility of hybrid offshore wind and tidal stream energy generation is worth further investigation.

(2) There is little research investigating the integration of a coastal community with hybrid offshore wind and tidal stream energy generation. Due to the maturity of technologies, solar PV and onshore wind are the two most frequently studied RE technologies in the field of ZEC. However, for a coastal community, there can be more combinations of the sources of energy generation, specifically, offshore wind and tidal stream in this study. Furthermore, it is noticed that most of the current studies on large-scale offshore wind and tidal stream energy development are focusing on the direct grid-connected systems and their cost of energy, while the system integration with a community is seldom discussed. As onsite generation is a vital element of a ZEC, it is important to discuss the RE generation and demand integrally.
(3) There is little research analysing the detailed RE generation characteristics and the corresponding system load matching of a ZEC. Most of the current studies on ZEC only compare the annual RE generation with the annual community demand and claim the community achieved zero energy. The detailed monthly and weekly characteristics of the RE generation and the corresponding dynamic system load matching are not analysed. However, it is suggested that the feasibility and suitability of developing a RE system should be further studied with dynamic simulation with the appropriate resolution, especially when the RE system is directly connected with the end-users. Thus, insights into the dynamic load matching and grid interaction can be provided.

It should be emphasized that these scientific gaps are summarized based on the literature review of the international research rather than the local studies. Therefore, these gaps are not constrained by a specific location, region, or climate condition. To address the above international scientific gaps, this study focuses on the detailed techno-economic feasibility investigation of a coastal ZEC supported by hybrid offshore wind and tidal stream energy generation. With the demonstration of a proposed case in Hong Kong, this study aims to:

(1) investigate the techno-economic feasibility of a coastal ZEC, which incorporates a hybrid offshore wind and tidal stream energy system for energy generation and an ocean and solar thermal energy supported district heating and cooling system for energy conservation.
(2) analyse the annual, monthly, and weekly energy generation characteristics of the hybrid offshore wind and tidal stream energy generation system, and subsequently, investigate the community system load matching. Further, the effectiveness of load matching enhancement by battery storage will be investigated.
(3) assess and compare the techno-economic performance and the equivalent carbon emission of the 21 proposed cases.

The results in this paper could provide important insights into the developments of ZECs and hybrid offshore wind and tidal stream energy generation systems worldwide, especially for other densely populated coastal cities with significant energy demand, such as Singapore, Mumbai, etc. The remaining sections of this paper are arranged as follow: Section 2 gives an introduction to the simulation environment, the proposed coastal community, and the relevant energy resource and weather profiles. Section 3 gives a detailed description of the TRNSYS modelling of the proposed community energy system. Section 4 introduces the framework of this study and the key performance indicators. Section 5 analyses the system performance from the technical, economic, and carbon emission perspectives. Section 6 concludes the important findings of the study.

2. The simulation environment, coastal community, and weather

2.1. Simulation environment

In this simulation-based study, TRNSYS 18 is used for assessing the dynamic performance of the community energy system. TRNSYS stands for Transient System Simulation Tool. It is a graphical software simulation tool that provides a flexible and transient system simulation environment. TRNSYS 18 consists of two major components – a computing engine and an extensive library. The computing engine builds the simulation input file based on the graphical system design, reads the input file, and subsequently, solves the simulation through iteration. It is capable of simulating the transient system performance in a fine resolution up to 8 time steps in an hour. In addition, the simulation cycle can be adjusted, allowing users to conduct not only short-term analysis but also long-term analysis that involves continuously changing system conditions throughout the operation cycle, for example, battery degradation. In this study, the simulation time step and simulation cycle are kept at 15 mins and 1 year, respectively. The annual system performance is considered the same throughout the operation cycle without addressing the system degradation. In addition, the extensive TRNSYS library contains a wide range of established models, including the critical models in this study, such as chiller, heat pump, heat exchanger, thermal storage tank, battery, etc. With the wide model coverage and the transient computing capability, TRNSYS 18 is widely used for simulating thermal and electrical energy systems [35].

2.2. The coastal community

To assess the techno-economic feasibility of a coastal ZEC with hybrid offshore wind and tidal stream energy generation, a coastal location in Hong Kong is selected for case study and demonstration. The proposed coastal community is set to be located at Ma Wan, Hong Kong, as depicted in Fig. 1. It has the size of a typical community with 8 high-rise residential buildings and 2 mid-rise office buildings. Each high-rise residential building has 40 floors above ground, and each mid-rise office building has 10 floors above ground and 1 underground parking floor. The residential buildings are modelled according to the layout plan of the standard block Harmony 1 (Option 1) by the Hong Kong Housing Authority [36]. Each residential floor has an area of 1152 m^2. The office buildings are modelled according to a typical office layout, which has a floor area of 480 m^2. The building envelops, the occupation schedules, and operation schedules of both buildings follow the Performance-based

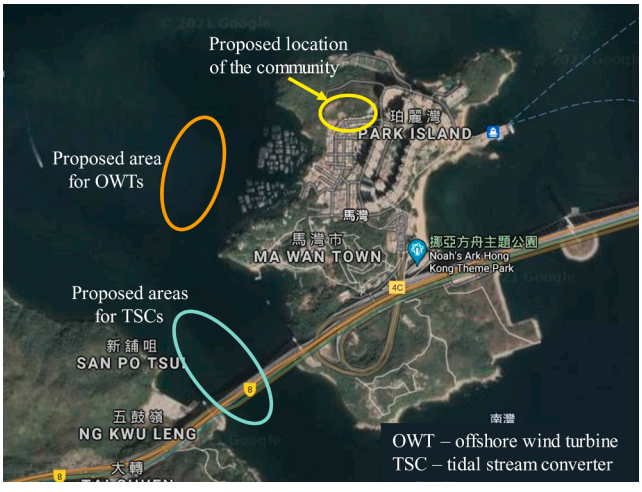

Fig. 1. The proposed location for the coastal community, tidal stream converters, and offshore wind turbines.

Building Energy Code (2007 Edition) and BEAM Plus New Buildings Guideline (version 1.2).

Table 1 and Table 2 list the annual demand energy and the annual demand peak power of several community services, including space cooling, air handling unit (AHU) cooling, space heating, AHU heating, domestic hot water (DHW) heating, and the basic electricity demand. The basic electricity demand comprises the lighting systems and other equipment. Fig. 2 illustrates the annual duration curve of the community. It is observed that the community demand is dominated by space cooling, AHU cooling, and basic electricity demand. Space cooling is the most demanding service – the annual space cooling demand energy is 188.86 kWh/m^2, and the annual space cooling demand peak power reaches 18.53 MW. On the other hand, although a relatively large annual heating demand peak power is observed, the demand energy of heating services is less significant, especially space heating, which is only required during 11.65% of the time in a year. It should be noticed that the demand of the community is calculated by directly aggregating the demand of each type of building. Therefore, it may result in a slight overestimation and a slight time shift from the actual community peak power in reality.

2.3. Weather

2.3.1. Seawater temperature profile

A 5-year average surface seawater temperature profile is acquired to simulate the performance of the indirect seawater cooled chillers and the direct sea-source heat pumps in the ocean and solar thermal energy supported district cooling and heating system. The surface seawater temperature is measured at the Waglan Island Observatory Station by the Hong Kong Observatory from 2013 to 2017. The measuring depth is 1 m, and the measuring interval is 1 h. Fig. 3 illustrates the average annual temperature profile and the wet-bulb temperature in Hong Kong. It can be observed that the surface seawater temperature is at a similar level as the wet-bulb temperature during June to August. While during the winter periods, the surface seawater temperature is noticeably lower. However, the surface seawater temperature is much more stable than the wet-bulb temperature throughout the year.

2.3.2. Offshore wind profile

The annual wind speed profile is obtained from the TRNSYS meteonorm weather database. The data measuring location is the King's Park Meteorological Station, and the data measuring height is 10 m above the ground. It should be mentioned that the King's Park Meteorological Station is close to the coastline. Therefore, although an onshore wind profile is used to estimate the offshore wind energy generation, the underestimation will be insignificant, because the proposed area for OWTs is at the nearshore region as depicted in Fig. 1. With the 10 m wind speed, the wind profile at the 65 m hub height can be calculated using the Wind Profile Power Law. The annual maximum and minimum wind speeds at 65 m height are 17.09 m/s and 0.13 m/s, respectively. The annual wind speed profile at the 65 m hub height and the corresponding spectrum are depicted in Fig. 4**(a)**. The annual wind speed occurring probability and the Weibull Distribution are presented in Fig. 4**(b)**. It is observed that the offshore wind speed is higher than 4 m/s during 68.89% of the time in a year and is higher than 10 m/s during only 8.01% of the time in a year. The most frequently occurring wind speeds fall in the range of 4–6 m/s. Furthermore, Fig. 4**(c)** presents the monthly average wind speed at 65 m height with the respective monthly maximum and minimum values. The highest monthly average wind speed 6.38 m/s occurs in March and April, closely followed by the 6.37 m/s in February and June. The lowest monthly average wind speed 4.03 m/s is observed in July. Moreover, the monthly maximum wind speed in July is significantly lower than the other months, corresponding to the darker wind pattern during day 181 to day 212 in Fig. 4**(a)**.

2.3.3. Tidal stream profile

The tidal stream velocity profile in 2017 is acquired from the Marine Department. The location of the tidal stream profile is at the water channel under the Kap Shui Mun Bridge, as indicated in Fig. 5. According to the Hong Kong Government [37], the tidal stream velocity profile is generated by a tidal prediction system, which utilizes the Hong Kong Tidal Atlas Model. The predicting interval is 15 mins. Fig. 6**(a)** presents the tidal stream speed pattern and demonstrates the periodic nature of tides in Hong Kong. It can be observed that tidal stream is most resourceful during the afternoon of spring and summer, and during the night of autumn and winter. Fig. 6**(b)** illustrates the occurring probability of the tidal stream speed. The tidal stream speed is higher than 0.5 m/s during 70.04% of the time in a year, and the most frequently occurring speeds fall in the range of 0.5–1 m/s. In addition, Fig. 6**(c)** shows the monthly average tidal stream speed at the surface seawater layer with the respective monthly maximum and minimum values. Due to the periodic occurring nature of tides, the tidal stream resource is more stable across the year compared to offshore wind. The largest monthly average speed of 0.81 m/s occurs in March, and the annual maximum tidal stream speed is 2.16 m/s.

3. The proposed community energy system

3.1. The basic components and the control principles

The schematic diagrams in Fig. 7 illustrate the main components of the proposed community energy system and the energy flows between. The system boundary is set at the interface with the electric grid, which is naturally left outside the system boundary as it falls on the scope of public utility. In addition, vehicles are excluded from the community energy system and not considered in this study. On the electricity side of the community energy system, OWTs and TSCs are the main power generators. Considering the intermittence of RE generation, the community energy system is connected with the grid to guarantee a reliable power supply. Because the instantaneous system load matching can hardly be controlled at 100% even with energy storage, there could be excessive RE generation exported to the grid and RE generation deficit that has to be compensated by importing electricity from the grid at any moment throughout the year. In this case, although grid interaction is unavoidable, the community is still considered a ZEC if the amounts of exported RE exceed the amounts of imported grid electricity. On the thermal energy side, the community energy system delivers chilled water and hot water to meet the cooling and heating demands. The chilled water and hot water are stored in the central cooling and heating tanks, in which the temperatures are maintained by a series of seawater cooled chillers, a sea-source heat pump, and solar thermal collectors. To guarantee the supply hot water reaches the desired temperature, electric heaters will heat the water before it is supplied to the end-users. Therefore, electricity is the sole energy carrier in the designed community energy system.

As illustrated in Fig. 7, the community energy system performance is

Table 1
Annual services demand energy of the coastal community (kWh/m^2).

	Space cooling	AHU cooling	Space heating	AHU heating	DHW heating	Basic electricity demand
Office building	38.22	223.38	0.39	6.04	4.47	191.28
Residential building	121.17	56.71	3.10	7.74	32.91	49.86
Community	118.86	61.35	3.02	7.69	32.12	53.80

Table 2
The services peak demand power of the coastal community (kW).

	Space cooling	AHU cooling	Space heating	AHU heating	DHW heating	Basic electricity demand
Office building	204.02	1,177.81	39.34	20.98	8.81	255.75
Residential building	2,316.73	1,024.15	1,006.20	71.40	556.80	689.18
Community	18,533.83	9,752.93	8,112.18	613.14	4,455.35	5,610.95

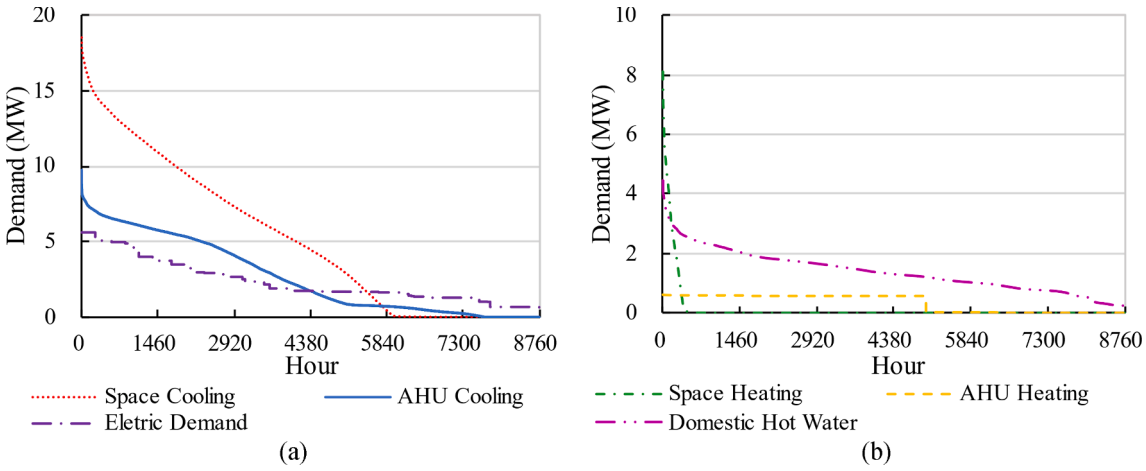

Fig. 2. Duration curves of the community demands.

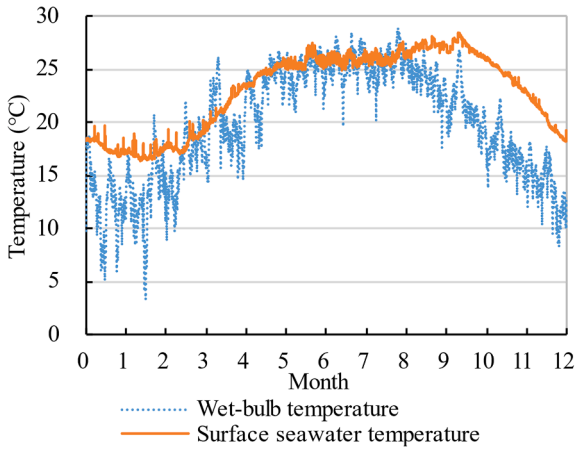

Fig. 3. Annual surface seawater temperature and wet-bulb temperature.

investigated under 2 scenarios – scenario 1 without battery storage and scenario 2 with battery storage. In scenario 1, the RE generation is prioritized to cover the community energy demand. Thereafter, the 1st stage RE surplus and 1st stage RE shortage will be exported to and imported from the electric grid. In scenario 2, a deep-cycle community-scale battery is integrated to enhance the system load matching. The maximum battery charging and discharging power are limited at 0.2C [38] for conservative reasons. Similar to scenario 1, the priority of RE utilization is to cover the community demand. However, when the RE generation exceeds the community demand, the 1st stage RE surplus will firstly be stored in the battery. In the situation where the battery storage is full or the 1st stage RE surplus exceeds the battery charging limit, the grid will accommodate the 2nd stage RE surplus. On the other hand, when the RE shortage exists, the battery will discharge electricity to fill the 1st stage RE shortage. If the battery discharging power is insufficient to cover the instantaneous community demand, the 2nd stage RE shortage will be imported from the grid.

3.2. The ocean and solar thermal energy supported district cooling and heating system

An ocean and solar thermal energy supported district cooling and heat system is developed to increase the energy efficiency of the community thermal conditioning system. The district cooling and heating system provides thermal conditioning services including AHU cooling, space cooling, AHU heating, and DHW. As space heating is only required during 11.65% of the time in a year, it is not provided in the district heating system.

During the TRNSYS system modelling processes, the indirect seawater cooled chillers are estimated with reference to the product catalogue "30XW – 30XWH" by Carrier. This chiller product is a highly energy-efficient model, which has a nominal cooling coefficient of performance (COP) of 6.08 and a part load performance European Seasonal Energy Efficiency Ratio of 7.18. As the district cooling and heating system is at the scale of a community, a relatively large chiller unit is selected, specifically, unit 1762 is selected for chiller modelling. The number of chillers required for AHU cooling and space cooling is determined according to the peak community cooling demand. For example, the cumulated nominal cooling capacity of the chillers in the AHU cooling system should exceed 70% of the annual peak community AHU cooling demand in Fig. 2**(a)** and Table 2. The 70% factor is introduced to avoid unnecessary oversizing that specifically targets the short-lasting annual peak demand. Similarly, the performance of the direct sea source heat pump is modelled according to the reversible heat pump unit 1312 in the catalogue. In addition, the seawater heat exchangers are modelled with a constant effectiveness of 0.7 for conservative reasons, as Sanaye and Hajabdollahi [39] suggested the practical effectiveness of plate-fin heat exchangers is between 0.7 and 0.8.

In the AHU cooling system, chilled water is supplied to the AHU cooling coils, where the heat exchange process occurs. In addition to sensible cooling, the AHUs will also extract the latent heat in the air and provide dehumidification through condensation, which requires a relatively low chilled water temperature – 7 °C in this case. According to the chiller sizing, 5 indirect seawater cooled chillers will be required to maintain the temperature of the AHU cooling storage tank. The AHU cooling storage tank has a storage capacity to sustain 1 h of the peak

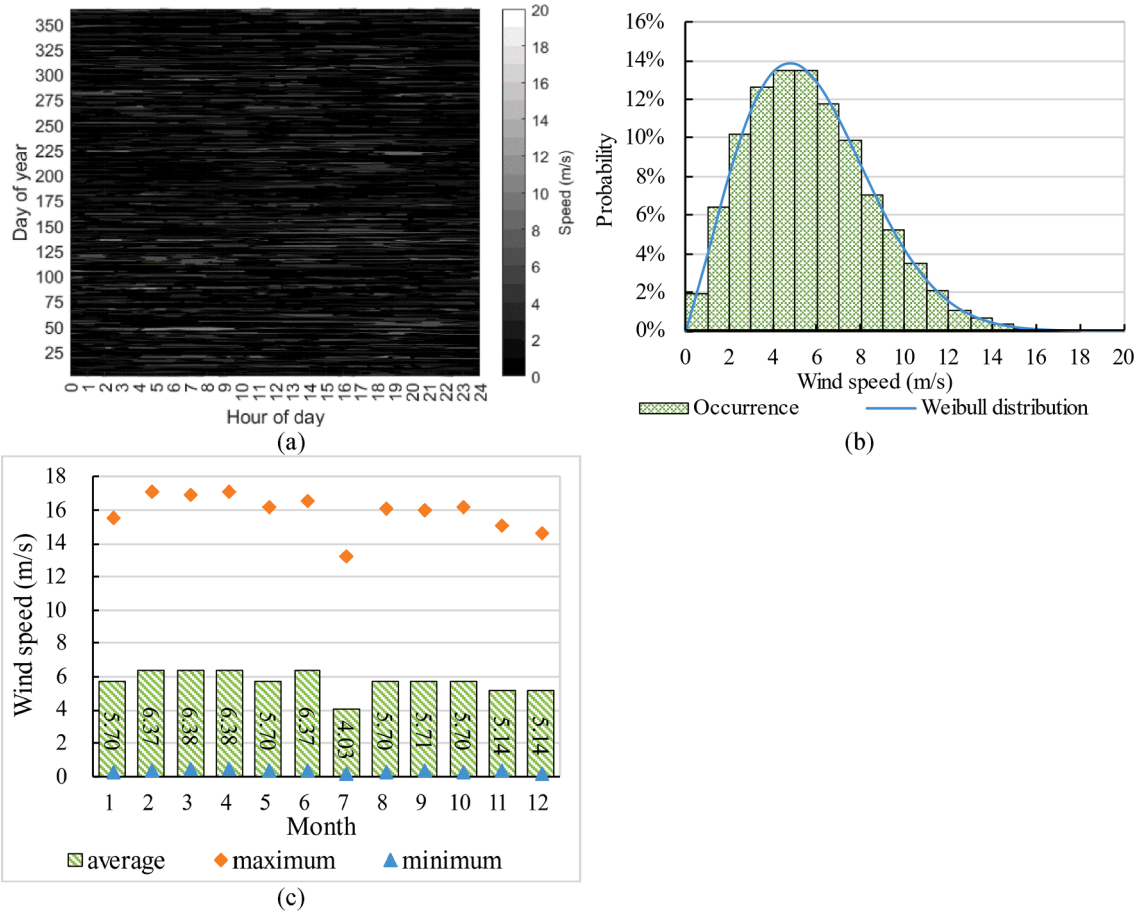

Fig. 4. (a) Carpet plot of annual wind speed at 65 m high; (b) Annual occurrence and Weibull distribution of wind speed at hub height (65 m); (c) Monthly wind speed profile at 65 m high.

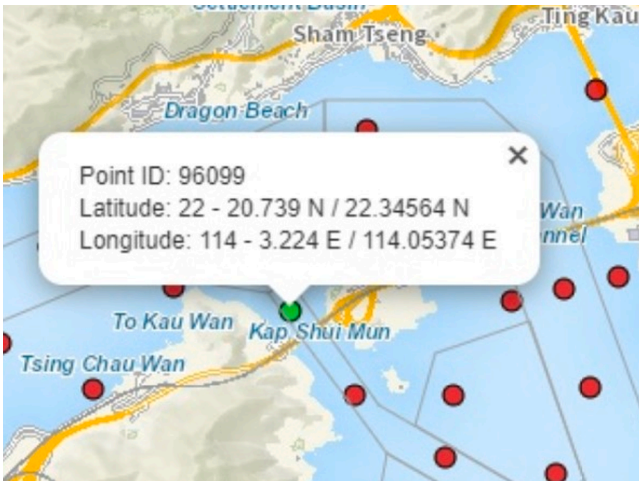

Fig. 5. The selected location for the tidal stream velocity profile.

AHU cooling demand. The storage temperature is 7 °C. When the storage temperature is higher than 7 °C, all of the 5 chillers will operate to recharge the storage tank and retain the storage setpoint. Considering the temperature stratification, the recharging chilled water is supplied to the bottom node of the cooling storage tank. As shown in Fig. 7, the storage tank serves as the intermediate point between the chilled water recharge loop and the chilled water supply loop. With the cooling buffer provided by the storage tank, the operation of chillers is isolated from the real-time community cooling demand. Therefore, the operation of the chilled water recharging loop, the chiller condenser loop, and the seawater loop is modelled with constant flow rates. However, to satisfy the instantaneous community cooling demand, the chilled water supply loop operates at the variable chilled water flow rate. Under the design conditions, the chilled water leaves the bottom node at 7 °C and returns to the top node at 12 °C with a 5 °C temperature difference.

Space cooling in the community is provided through chilled beams, which operate at a higher temperature than the AHU cooling system. Specifically, the supply temperature for space cooling is 15 °C and the return temperature is 17 °C. According to the Reversed Carnot Cycle, the COP of heat pumps is directly affected by the evaporating temperature. With the higher chilled water temperature, it is expected that the COP of the space cooling system will be higher than the AHU cooling system. The configuration of the space cooling system resembles the AHU cooling system. The major differences are the numbers of chillers, the storage temperature, the storage tank size, as well as the temperature and flow rate in each water loop. With the same sizing method as the AHU cooling system, 8 chillers are required in the space cooling system. Similarly, the space cooling storage tank has a storage capacity to sustain 1 h of the peak space cooling demand. As the space cooling chillers operate with a constant flow rate, the 5 °C temperature difference should be maintained at the inlet and outlet of the evaporator. As the return water temperature is 17 °C, the chilled water temperature at the outlet of the evaporator will be 12 °C, which is therefore set as the cooling storage temperature. A tempering valve is inserted between the chilled water supply and return branches so that a portion of the returning chilled water can be diverted to mix with the 12 °C chilled water to satisfy the 15 °C chilled water supply temperature.

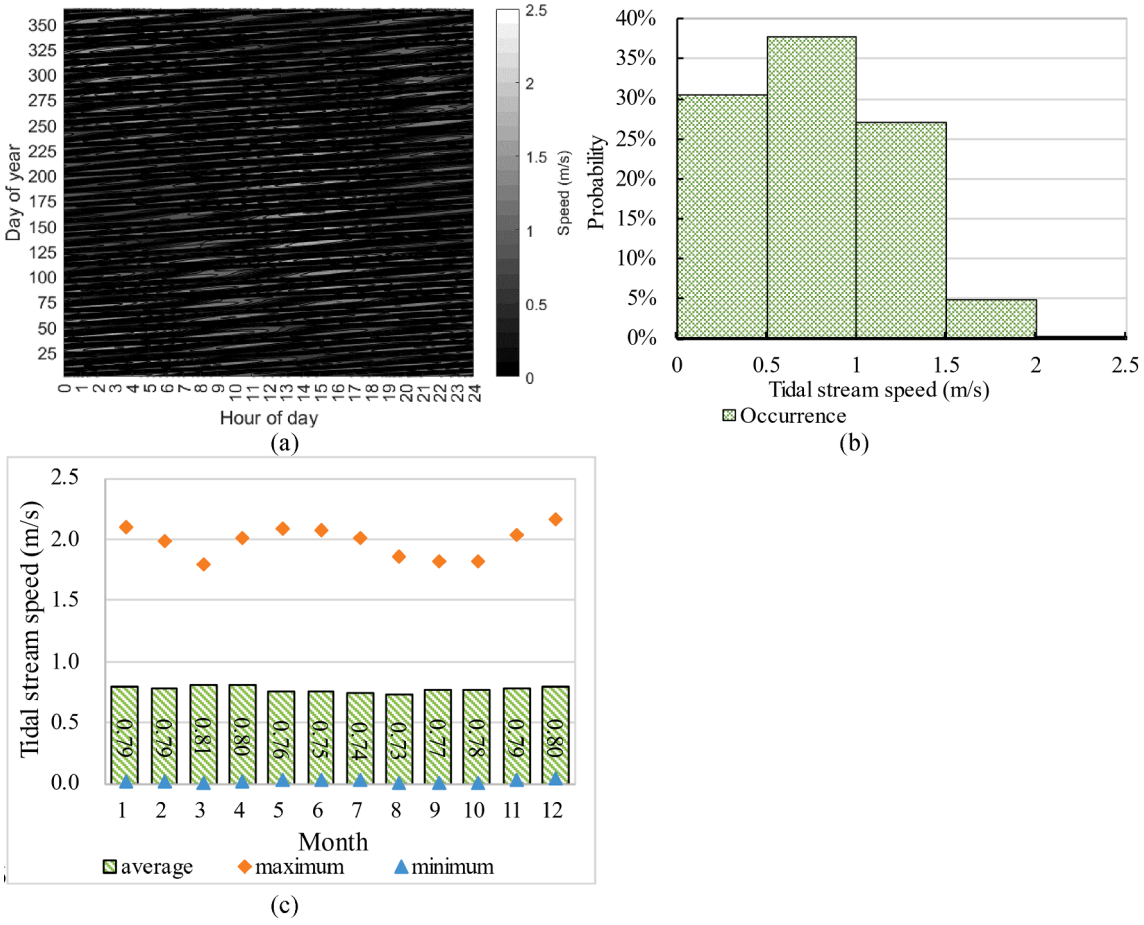

Fig. 6. (a) Carpet plot of annual tidal stream speed; (b) Annual occurrence of tidal stream speed; (c) Monthly tidal stream speed profile.

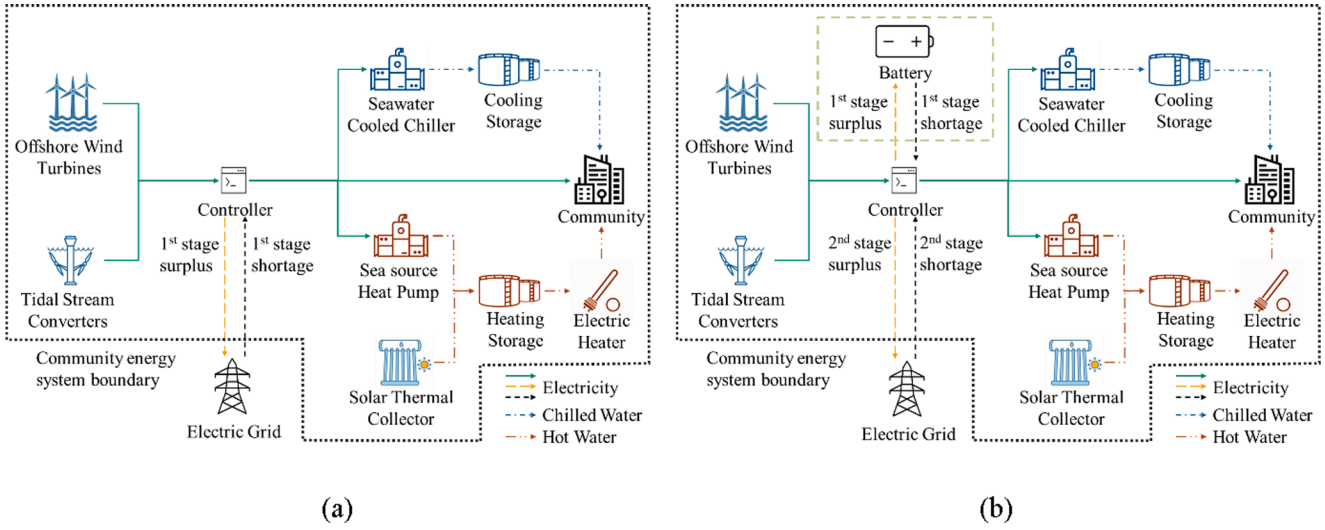

Fig. 7. Community energy system schematics (a) Scenario 1 without battery; (b) Scenario 2 with battery.

The AHU heating system and DHW system are compacted together by sharing the same heating storage tank. The heating storage tank is able to sustain 2 h of the combined peak heating demands. The solar thermal collectors and the direct seawater heat pump are two major heat sources for the heating storage tank. To increase the system energy efficiency, solar thermal collectors are prioritized as the primary heat source. It is assumed that approximately 10% of the total community roof area (i.e., 1000 m^2) is covered by solar thermal collectors. Thereafter, the direct seawater heat pump will increase and maintain the storage temperature at 50 °C. The supply and return temperatures in the AHU heating loop are set at 40 °C and 30 °C, respectively. While the supply temperature of DHW is set at 55 °C. As the reversible heat pump is only capable of providing mid-temperature heating approximately up to 50 °C. Electric heaters at the supply loops will raise the hot water

temperature to the supply temperatures.

3.3. The hybrid renewable energy system

3.3.1. Offshore wind turbines

To enable the case study with different combinations of OWT and TSC, an OWT with a medium generation capacity and a reasonable capacity factor is preferred. In this case, the 2 MW OWT (HTW2.0–80) manufactured by Hitachi Ltd. [40] is chosen for estimating offshore wind energy generation. The downwind OWT has a rotor diameter of 80 m and a swept area of 4978 m^2. The hub is located at 65 m high. Furthermore, the cut-in speed of the OWT is 4 m/s, and the rated power output is achieved at a wind speed of 13 m/s. Fig. 8 depicts the power curve of the 2 MW OWT. With reference to the wind speed probability in Fig. 4**(b)**, the OWT will operate during 68.89% of the time in a year. However, the rated power output is reached during only 1.82% of the operating time. In TRNSYS 18, the component model Type 90 is used for modelling the OWT. According to the annual energy consumption of the community, at least 10 OWTs are required to generate sufficient RE to achieve zero-energy in case 1, forming a 20 MW offshore wind farm. The 20 MW offshore wind farm will generate 37.16 GWh electricity annually with a 21.21% capacity factor. As 10 OWTs are required to generate sufficient energy in case 1, 10 other cases with different numbers of OWTs can be formed with the additional TSCs. Therefore, 9 hybrid RE cases and 2 single RE cases can be formed, enabling a systematic case study and the comparison between different systems.

3.3.2. Tidal stream converters

The Neptune NP1000 floating TSC developed by Neptune Renewable Energy Ltd. is selected to estimate the tidal stream energy generation. The TSC contains a 6 m × 6 m vertical crossflow turbine with a 250 kW rated capacity. The overall dimensions of the TSC are 20.0 m × 12.8 m × 6.5 m (L × W × D) [41]. Compared to other axial-flow TSCs with similar rated capacities, for example, a 300 kW horizontal-axis TSC with a radius of 8.5 m [42], the Neptune NP1000 has a relatively small size. Thus, it is considered more suitable for the applications at shallow nearshore environments, especially at the selected water channel under the Kap Shui Mun Bridge, where bathymetry by the Marine Department shows the seawater depth between 20 m and 30 m. Moreover, according to Roberts et al. [8], crossflow turbine is the most suitable type of TSC for nearshore applications because of the high power density and the less stringent requirement on the water depth. In addition, the Neptune NP1000 is equipped with a Venturi duct which accelerates the entering tidal stream. Therefore, the Neptune NP1000 can operate at locations with relatively low tidal stream speeds. Specifically, it produces the 250 kW rated power at a 3 m/s tidal stream speed, while only requiring a 0.5 m/s cut-in speed, which is 16.67% of the rated tidal stream speed. Compared to a standardised horizontal TSC that typically requires a cut-in speed at 30% of the rated speed [9], the Neptune NP1000 has a relatively low cut-in speed requirement, and thus, has higher potential in generating tidal stream energy under low-speed environments. With reference to the tidal steam speed occurring probability in Fig. 6**(b)**, the Neptune NP1000 will operate during 70.04% of the time in a year.

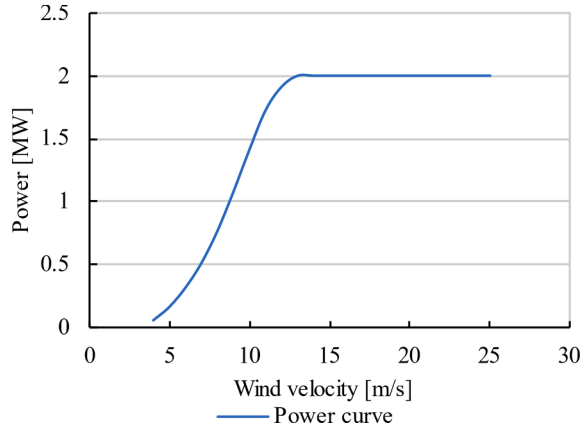

Fig. 8. The power curve of the 2 MW OWT.

According to Hardisty [41], the power output from a TSC or marine current turbine can be approximated by a generalized logistic function in Eq. (1).

$$P(t) = \frac{K}{(1 + Qe^{-B(U(t)-M)})^{1/y}} \quad (1)$$

where $P(t)$ and $U(t)$ are the instantaneous power output and the tidal stream velocity, respectively. K is the upper asymptote, which represents the installed capacity of the TSC. Q is a value that depends upon the turbine design. B is the rate of power increase. M is the tidal stream velocity at which the maximum power increase happens. y is the symmetry of increase, affecting where the maximum power increase occurs. In addition, Hardisty [41] conducted a series of dock tow trial experiments to verify the modelling method. The experiment results showed reasonable approximation compared to the commercial power curve and proved the modelling legitimacy. In this paper, a generalized logistic function is fitted to predict the RE generation according to the power characteristics listed in Table 3 [41]. Fig. 9 shows the fitted power curve, and Table 4 summarizes the fitted value of each variable. According to the simulation result, 291 TSCs with a total system capacity of 72.75 MW are required to generate a similar amount of RE as the 20 MW offshore wind farm. The significant system capacity difference is caused by "the effectiveness of energy generation". To be specific, the TSC utilizes less than or equal to 26.8% of the full capacity during 92.65% of the operating time. On the other hand, the OWT utilizes less than or equal to 25.80% of its full capacity during only 56.20% of the operating time. In other words, the TSC has a much smaller capacity factor (5.55%) than the OWT.

4. Methodologies

4.1. Research framework

To comprehensively investigate the potential of the offshore wind and tidal stream RE systems, 21 cases are formed and classified into 2 groups. The RE systems in each case are assembled by a unique combination of OWTs and TSCs, as listed in Table 5. The 11 cases in group 1 will generate similar amounts of RE annually, and the 11 cases in group 2 have the same generation capacity. According to the community demand profile, at least 10 OWTs (the 20 MW offshore wind farm in case 1) or 291 TSCs (the 72.75 MW TSC array in case 11) are required to generate sufficient energy to cover the annual community energy consumption. The significant capacity difference between case 1 and case 11 is caused by the lower generation effectiveness of the TSC, as mentioned in Section 3.3.2. Nine hybrid RE cases with a similar annual RE generation are established in group 1. It should be noticed that the annual RE generation in group 1 will be larger than the annual community energy consumption. The exceeding generation is used to cover the possible energy loss induced by power conversion, battery charging, etc. In addition, 10 additional cases which have the same generation capacity as case 1 are formed and classified into group 2.

A reference case is developed to reflect the economic performance of the proposed community energy system and to demonstrate the level of energy conservation achieved by the ocean and solar thermal energy

Table 3
Power characteristics of the Neptune NP1000.

Tidal stream velocity (m/s)	0.51	1.02	1.53	2.04	2.55	3.06
Power output (kW)	2	13	67	178	236	250

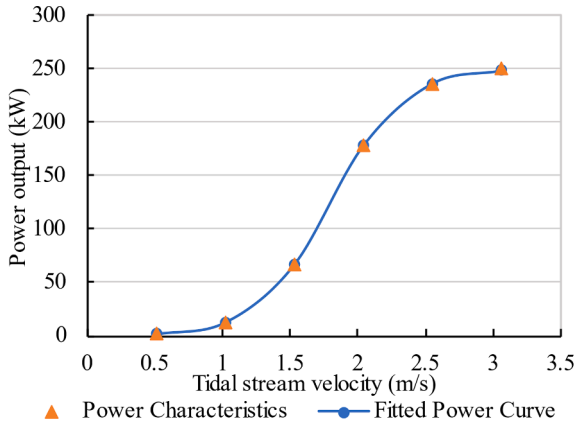

Fig. 9. The fitted power curve of the Neptune NP 1000.

Table 4
Parameters for the fitted generalised logistic function of the Neptune NP1000.

Parameter		Value
K	Upper asymptote set to the installed capacity (kW)	250
Q	Depends upon turbine design	5.785
B	Rate of power increase	0.122
M	Maximum increase	1.3306
Y	Symmetry of increase	0.0325

Table 5
Summary of the 21 RE systems.

Group	Case	NO. of OWT	NO. of TSC	System Capacity (MW)	Generation (million kWh)	Demand (million kWh)
Group 1 & 2	**1**	10	0	20.00	35.30	34.69
Group 1	**2**	9	30	25.50	35.42	
	3	8	59	30.75	35.41	
	4	7	88	36.00	35.41	
	5	6	117	41.25	35.40	
	6	5	146	46.50	35.39	
	7	4	175	51.75	35.39	
	8	3	204	57.00	35.38	
	9	2	233	62.25	35.37	
	10	1	262	67.50	35.37	
	11	0	291	72.75	35.36	
Group 2	**12**	9	8	20.00	32.75	
	13	8	16	20.00	30.19	
	14	7	24	20.00	27.63	
	15	6	32	20.00	25.07	
	16	5	40	20.00	22.51	
	17	4	48	20.00	19.95	
	18	3	56	20.00	17.40	
	19	2	64	20.00	14.84	
	20	1	72	20.00	12.28	
	21	0	80	20.00	9.72	

supported district cooling and heating system. In the reference case, the chiller condensing heat is dissipated through freshwater cooling towers, and all of the heating demands are covered by electric heaters. Therefore, same as the proposed community energy system, electricity is the sole energy carrier.

The research steps in this study are illustrated in Fig. 10. Firstly, the energy-saving potential of the ocean and solar thermal energy supported district cooling and heating system is evaluated in Section 5.1. Secondly, the technical performance of group 1 scenario 1, as shown in Fig. 7**(a)**, is discussed in Section 5.2.1 with the detailed monthly and weekly system analysis. Thirdly, the technical performance of group 2 scenario 1, as shown in Fig. 7**(a)**, is briefly discussed in Section 5.2.2. Fourthly, the technical impacts of the community-scale battery are investigated in Section 5.2.3 by analysing the technical performance of group 1 scenario 2, as shown in Fig. 7**(b)**. The techno-economic analysis of the 21 cases is introduced in Section 5.3. Three FiT situations are evaluated in the techno-economic analysis, namely the generation based FiT_1, export FiT_2, and no FiT. Sensitivity analysis is conducted to discuss the uncertainties associated with the chosen capital investment costs in Section 5.4. Lastly, Section 5.5 briefly discussed two additional options for achieving a ZEC, namely, a rooftop PV system and generation of RE in remote areas.

4.2. Analysis criteria

4.2.1. Technical performance

To quantify the technical performance of the community energy system, two basic load matching indices – onsite energy matching (OEM) and onsite energy fraction (OEF) are chosen. According to Cao, Hasan, and Siren [43], OEM represents the RE self-consumption ratio, which measures the proportion of RE generation used to cover the energy consumption rather than dumped or exported. OEF represents the load coverage ratio, which measures the proportion of energy consumption covered by the onsite RE generation rather than imported from the grid. Therefore, the higher values of OEM and OEF denote better system load matching during the specified period. As the community-scale battery is integrated in scenario 2 to improve the system load matching, the enhancement of OEM and OEF will represent the RE shifting ability provided by the battery. The calculations of OEM and OEF can be simplified as Eqs. (2) and (3):

$$OEM = 1 - \frac{\int_{t_1}^{t_2} E(t)dt}{\int_{t_1}^{t_2} G(t)dt}; 0 \le OEM \le 1 \tag{2}$$

$$OEF = 1 - \frac{\int_{t_1}^{t_2} I(t)dt}{\int_{t_1}^{t_2} L(t)dt}; 0 \le OEF \le 1 \tag{3}$$

where $E(t)$, $G(t)$, $I(t)$, and $L(t)$ represents the instantaneous exported power, the instantaneous RE generation, the instantaneous imported power, and the instantaneous community demand, respectively.

4.2.2. Economic performance

For the economic analysis, the relative net present value (NPV_{rel}) and the relative discounted payback period (DPP_{rel}) are adopted to compare the market competitiveness of the systems. It should be mentioned that the economic performance in this study is evaluated relative to the reference case introduced in 4.1. Therefore, the results denote the net present value and the discounted payback period of the additional system investment. Moreover, cash flow with a positive value indicates income, while cash flow with a negative value indicates expenditure. The economic performance of the community energy system is investigated under three FiT situations – the generation based FiT_1, export FiT_2, and no FiT. FiT_1 calculates the subsidy based on the annual RE generation. Such RE generation based FiT has been imposed in Hong Kong since 2018 for solar PV and wind projects [44]. In this study, it is assumed that the FiT_1 covers both offshore wind and tidal stream energy systems without limitation on the system capacity. In addition, it is assumed that the 3 HKD/kWh FiT incentive in [44] will be extended after 2033, and the 20-year operation cycle of the community energy system will be fully covered. Therefore, the annual subsidy benefited from the FiT_1 can be calculated by Eq. (4):

$$B_{FiT,n} = FiT_1 \times E_{generation,n} \tag{4}$$

where $B_{FiT,n}$ is the annual FiT subsidy in the year n, and $E_{generation,n}$ is the annual RE generation in the same year.

FiT_2 is the export FiT scheme that measures the amount of RE exported to the grid. In this situation, the tariff rate FiT_2 is assumed same as the electricity tariff. According to the CLP Power Hong Kong Limited,

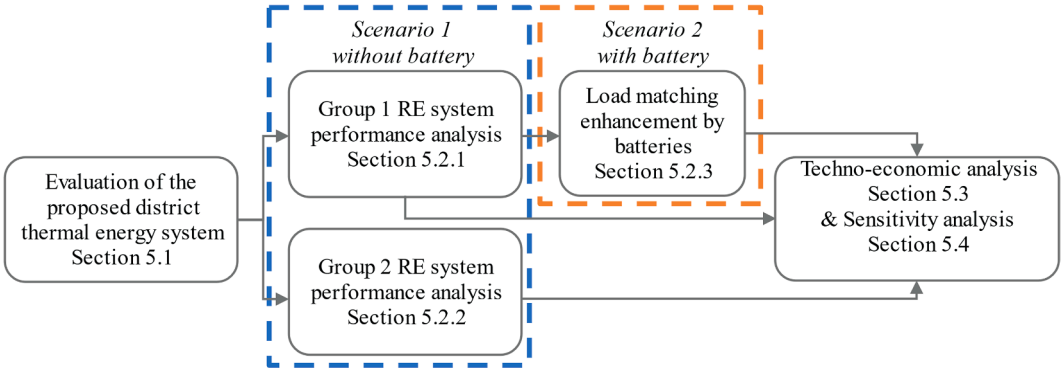

Fig. 10. Research steps and section flowchart.

the electricity tariff in 2021 is fixed at 1.218 HKD/kWh [45]. Therefore, the annual subsidy benefited from the FiT_2 can be calculated as Eq. (5):

$$B_{FiT,n} = FiT_2 \times E_{export,n} \tag{5}$$

where $E_{export,n}$ represents the annual RE exported to the grid in the year n.

In addition, compared to the reference case, the annual saving from operating the community energy system during the year n can be calculated by Eq. (6):

$$B_{saving,n} = C_{tariff} \times \left(E_{import,n,ref} - E_{import,n}\right) + \left(C_{O\&M,n,ref} - C_{O\&M,n}\right) \tag{6}$$

where C_{tariff} is the electricity tariff. $E_{import,n,ref}$ and $E_{import,n}$ are the annual imported energy of the reference case and the studied cased in the year n. $C_{O\&M,n,ref}$ and $C_{O\&M,n}$ are the annual operation and maintenance cost of the reference case and the studied case in the year n.

Thereafter, the NPV_{rel} of the community system during the 20-year operation cycle can be calculated by Eq. (7):

$$NPV_{rel} = -\left(C_{CAPEX} - C_{CAPEX,ref}\right) + \sum_{n=1}^{20} \frac{B_{FiT,n} + B_{saving,n}}{(1+i)^n} \tag{7}$$

where NPV_{rel} is the system NPV relative to the reference case. $C_{CAPEX,ref}$ and C_{CAPEX} are the capital investment cost of the reference case and the studied case. i is the interest rate. The DPP_{rel} is the first time point where the NPV_{rel} is balanced or positive.

4.2.3. Carbon emission

The equivalent CO_2 emission of the community energy system is calculated by the equivalent greenhouse gas emission factor (CEF_{eg}). According to the 2020 sustainability report by the CLP Power Hong Kong Limited, the greenhouse gas emission factor in 2020 is 0.37 kg CO_2e/kWh [46]. Therefore, the annual equivalent CO_2 emission (CO_2e) can be calculated by Eq. (8):

$$CO_2e = CEF_{eg} \times E_{import,n} \tag{8}$$

5. Simulation results and discussion

5.1. Technical impacts of the ocean and solar thermal energy supported district cooling and heating system

The performance of the reference case thermal energy system and the proposed district cooling and heating system is summarized in Table 6. It is noticed that there is only a slight chiller performance advantage in the proposed district system over the reference case. The AHU chillers in the proposed system achieve a 7.78 chiller COP, which resembles the reference case. Moreover, the space cooling chillers in the proposed system achieve an 8.61 chiller COP, which is mildly higher than the 8.44 chiller COP in the reference case. However, a noticeable difference can be found regarding the cooling system performance. The higher system efficiency achieved in the indirect seawater cooled district cooling system is mainly contributed by the less power demanding seawater pumps than the freshwater cooling tower fans. Given the higher energy efficiency, the annual AHU cooling energy consumption and the space cooling energy consumption are reduced by 13.20% and 13.37%, respectively. Furthermore, the proposed heating system achieves a 2.75 annual heating system COP. Compared to the reference case, the proposed system significantly reduces the annual heating energy consumption and the peak heating power by 71.40% and 51.48%, respectively. Moreover, the solar thermal collectors can cover 5.13% of the heating demand with a 52.07% annual solar efficiency. While the direct sea-source heat pump and the electric heaters contribute to the other 78.23% and 16.64% of the annual heating demand, respectively. Due to the significant heating energy saving, the average community energy use intensity is lowered by 26.21% from 123.99 kWh/m^2 to 91.49 kWh/m^2. In addition, the community peak power is lowered by 19.58% from 12.26 MW to 9.86 MW.

Table 6
Annual performance of the community thermal system.

	Indicators	Reference case	Proposed system
AHU cooling system	Chiller COP	7.78	7.78
	System COP	5.73	6.61
	System energy consumption (MWh)	4,082.76	3,543.66
	System peak power (kW)	1,686.31	1,431.73
Space cooling system	Chiller COP	8.44	8.61
	System COP	6.11	7.05
	System energy consumption (MWh)	7,419.86	6,427.62
	System peak power (kW)	3,229.23	2,795.52
Heating system	System COP	/	2.75
	System energy consumption (MWh)	15,116.81	4,323.74
	System peak power (kW)	4,357.69	2,114.45
Community	EUI (kWh/m^2)	123.99	91.49

- System COP is defined as the ratio of the useful thermal energy produced by chillers or heat pumps to the total cooling or heating system energy consumption, including the consumption by pumps, fans, etc.

5.2. Technical impacts of the combinations of hybrid renewable energy generation

5.2.1. Technical impacts of generation-based combinations (Group 1 scenario 1)

The annual system load matching of group 1 scenario 1 is summarized in Fig. 11**(a)** and Table 7. It can be found that the hybrid RE cases generally have better system load matching than the 2 single RE cases. Especially, case 5 has the best annual load matching, with a 56.68% OEM and a 57.84% OEF. It indicates that 56.68% of the hybrid RE

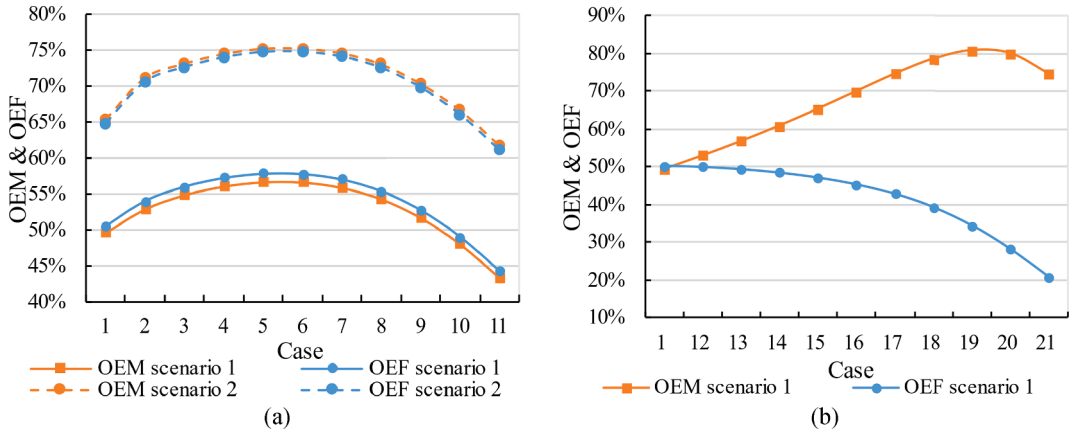

Fig. 11. Annual system load matching (a) group 1; (b) group 2.

Table 7
Summary of the annual technical performance and equivalent CO_2 emission.

Group	Case	Scenario 1 (without batteries)			Scenario 2 (with batteries)			
		OEM	OEF	CO_2e (kg/m^2)	Battery Capacity (MWh)	OEM	OEF	CO_2e (kg/m^2)
Group 1 & 2	**1**	49.61%	50.48%	16.76	92	65.38%	64.78%	11.92
Group 1	**2**	52.89%	54.00%	15.57	123	71.19%	70.59%	9.96
	3	54.88%	56.01%	14.89	107	73.19%	72.65%	9.26
	4	56.09%	57.24%	14.48	89	74.52%	74.00%	8.80
	5	56.68%	57.84%	14.27	70	75.25%	74.75%	8.55
	6	56.65%	57.79%	14.29	54	75.26%	74.77%	8.54
	7	55.91%	57.03%	14.55	43	74.60%	74.10%	8.77
	8	54.32%	55.39%	15.10	34	73.08%	72.55%	9.29
	9	51.72%	52.73%	16.00	27	70.37%	69.80%	10.22
	10	48.05%	48.98%	17.27	23	66.66%	66.02%	11.50
	11	43.36%	44.19%	18.89	20	61.78%	61.06%	13.18
Group 2	**12**	53.16%	50.17%	16.87				
	13	56.96%	49.56%	17.07				
	14	61.07%	48.63%	17.39				
	15	65.47%	47.31%	17.84				
	16	70.13%	45.50%	18.45				
	17	74.73%	42.98%	19.30				
	18	78.69%	39.46%	20.50				
	19	80.98%	34.63%	22.13				
	20	80.17%	28.38%	24.25				
	21	74.75%	20.94%	26.76				

- CO_2e of the reference case is 45.88 kg/m^2.

generation is consumed onsite, and 57.84% of the community energy demand is directly covered by the RE generation. Moreover, the ZEC is independent on the grid during 40.88% of the time in a year. Although the single RE case 1 and case 11 have inferior system load matching than case 5, the comparison between case 1 and case 11 reveals the better system load matching when the community energy system is supported solely by offshore wind energy generation. Quantitatively, case 1 achieves a 49.61% OEM and a 50.48% OEF, and the ZEC is independent on the grid during 37.76% of the time in a year. On the other hand, case 11 achieves a 43.36% OEM and a 44.19% OEF, and the ZEC is self-sufficient during 30.74% of the time in a year.

To analyse the system performance more comprehensively, the monthly offshore wind energy generation in case 1 is depicted in Fig. 12 **(a)**. The monthly offshore wind energy generation fluctuates. Especially in July, there is a significant offshore wind energy generation shortage. Comparatively, the monthly tidal stream energy generation in case 11 is more stable due to the periodic characteristics of tides, as depicted in Fig. 12**(b)**. While both cases generate more RE in a year than the annual community energy consumption, their monthly generation patterns do not comply with the monthly energy consumption pattern, whose peak and valley occur in July and February, respectively. Therefore, the ZEC is more dependent on the electric grid during the summer period, due to the higher energy consumption and because of the mismatch between the generation and the community demand. Specifically, in both case 1 and case 11, the peaks of the monthly imported energy peak occur in July, during which the lowest monthly OEF values are observed. In addition, although the monthly generation of the tidal stream energy is relatively steadier than the offshore wind energy, the monthly load covering ability of case 11 is worse than case 1 throughout the year except for July, November, and December.

In terms of hybrid RE systems, Fig. 12**(c)** illustrated the monthly hybrid RE generation of case 5. It shows that the hybrid RE generation is able to relieve the significant offshore wind energy generation shortage during July. Moreover, compared to case 1 and case 11, case 5 effectively reduces the grid interaction throughout the year, meaning that the system load matching is significantly enhanced. The system load matching enhanced by the hybrid RE cases is primarily contributed by the complementary generation pattern between offshore wind energy

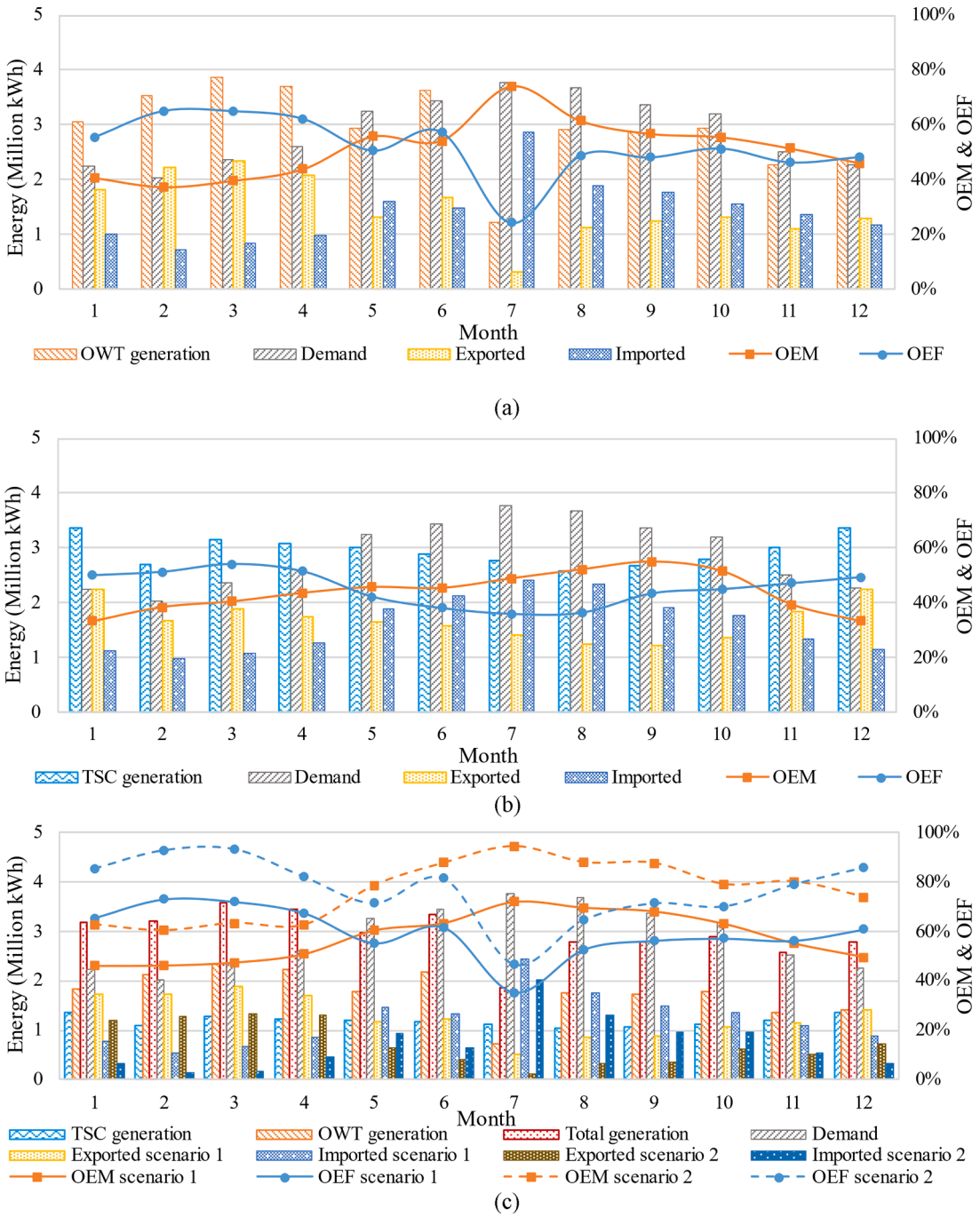

Fig. 12. Monthly system technical performance (a) case 1 scenario 1; (b) case 11 scenario 1; (c) case 5 scenario 1 and scenario 2.

and tidal stream energy during some specific periods. The complementary generation pattern can be visualized in Fig. 13, which depicts the RE generation, the community demand, and the RE coverage of the 3 aforementioned cases during the third week of June. During day 4 and day 5, a substantial offshore wind energy generation surplus is observed in case 1 and a substantial tidal stream energy generation shortage is observed in case 11. However, these RE surplus and shortage are balanced by the hybrid RE generation in case 5, which effectively shaves the spikes of the offshore wine energy generation in case 1 and fills the valleys of the tidal stream energy generation in case 11. Subsequently, the daily system load matching is improved.

5.2.2. Technical impacts of capacity-based combinations (Group 2 scenario 1)

The annual RE generation of group 2 scenario 1 is tabulated in Table 5, with the corresponding annual system load matching summarised in Table 7 and Fig. 11**(b)**. When the RE system capacity is fixed at 20 MW, the annual RE generation decreases linearly with the increasing proportion of TSCs. It is found that cases 12 to 21 fail to generate sufficient RE to cover the annual community energy consumption, and subsequently, fail to achieve the target of a ZEC. The OEF in group 2 has a negative correlation with the capacity of TSCs, indicating the decreasing system load covering capability as the proportion of TSCs increases. Meanwhile, the RE self-consumption ratio OEM firstly increases as the proportion of TSCs increases. The highest OEM value of 80.89% is achieved in case 19. However, the high OEM value does not

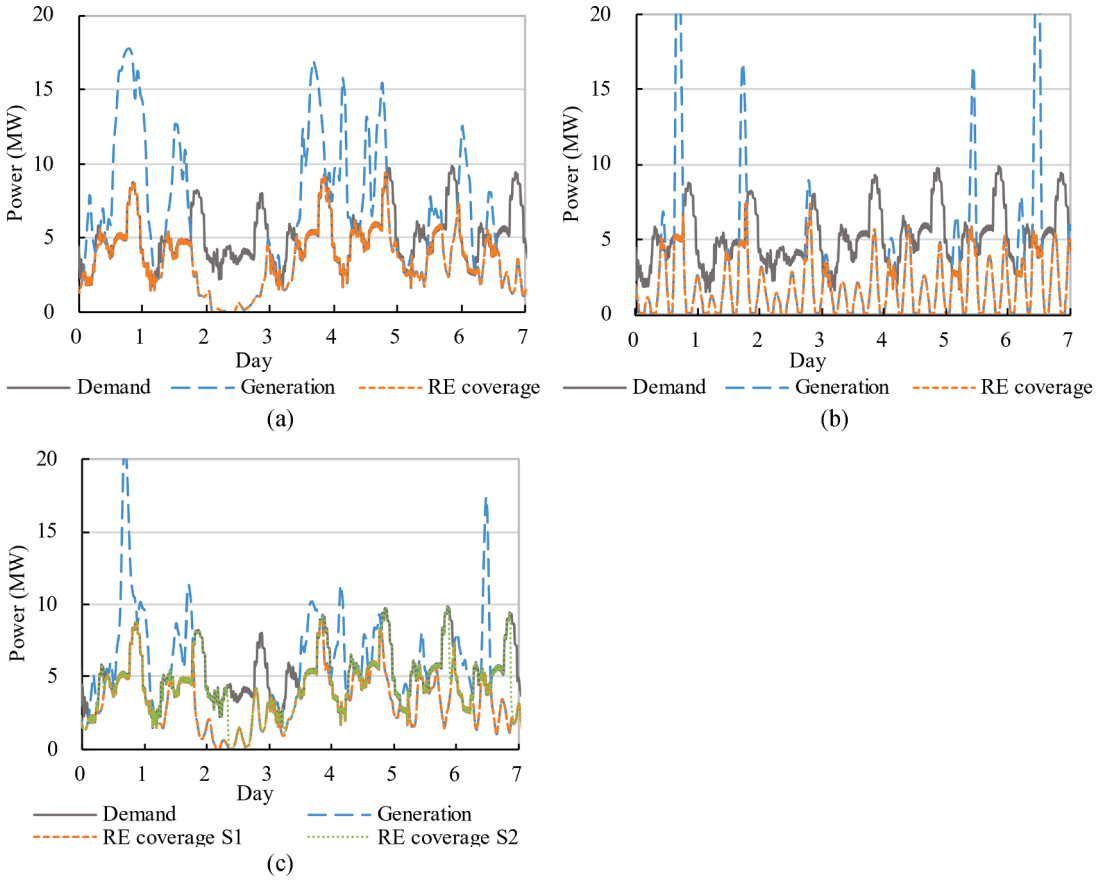

Fig. 13. Weekly system technical performance during the 3rd week of June (a) case 1 scenario 1; (b) case 11 scenario 1; (c) case 5 scenario 1 and scenario 2.

necessarily represent a good system technical performance, as the ultimate target is to achieve zero energy while minimising the grid interaction concurrently. In case 19, although 80.89% of the RE generation is consumed onsite, the grid interaction is not effectively reduced, and the community is still heavily relying on the grid imported energy to cover the energy demand. Since most of the cases in group 2 fail to achieve the target of zero-energy while not effectively reducing the grid interaction at the same time, the investigation on improving the system loading matching in Section 5.2.3 will focus on the 11 cases in group 1.

5.2.3. The solution to enhance the system matching capability (Group 1 scenario 2)

This study adopts the community-scale Li-ion battery as the solution to enhance the system load matching. Table 7 lists the determined battery capacity in each case and the corresponding system technical performance. During the TRNSYS system modelling, a 90% battery charging efficiency is considered. It is found that enlarging the battery capacity will increase the battery charging loss, and subsequently reduce the exported energy. Therefore, continuously increasing the battery capacity will eventually reach a turning point where the excessive annual RE generation is cancelled by the battery charging loss. At the same turning point, the imported energy is balanced with the exported energy. In other words, the coastal community is at the limit of achieving net-zero energy. Therefore, the battery capacity in each case is determined at the turning point, so that the technical performance enhancement can be maximised without compromising the target of achieving net-zero energy.

The system load matching of group 1 is noticeably increased in scenario 2, and all of the 9 hybrid RE cases have better system load matching compared to case 1 and case 11. Specifically, case 6 has the best annual technical performance with an OEM of 75.26% and an OEF of 74.77%. In case 5, the OEM and OEF are also increased significantly to 75.25% and 74.75%. The grid-independent period of case 5 is increased from 40.88% to 64.59% of the time in a year. Moreover, the monthly system load matching is noticeably enhanced, while the monthly grid interaction is substantially reduced, as illustrated in Fig. 12**(c)**. In addition, the enhanced system load matching and additional RE shifting ability provided by the community-scale battery can be visualized in Fig. 13**(c)**, which depicts the weekly system load matching profile of case 5 during the third week of June. Fig. 14 illustrates the corresponding weekly dynamic grid interactions, the battery charging and discharging processes, and the battery fraction state of charge (FSOC). On day 1, the battery stores the 1st stage RE surplus until the higher limit

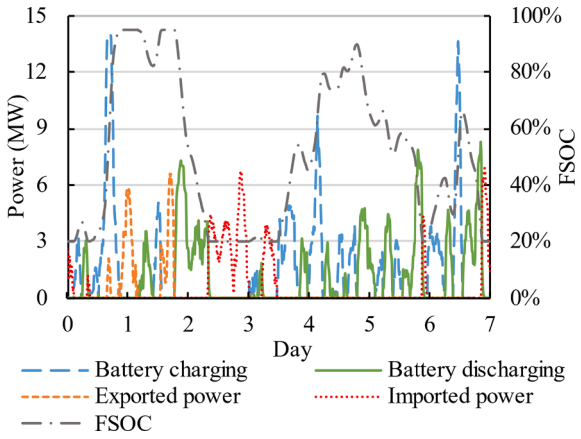

Fig. 14. Weekly battery power flows and grid interaction of case 5 scenario 2 during the 3rd week of June.

of FSOC is reached. On day 2 and day 3, the RE storage is released by the battery to cover the 1st stage RE shortage until the lower limit of FSOC is reached. Thereafter, the RE shortage during day 3 is filled by the imported electricity. It should be mentioned that the imported power in scenario 1 can be represented by the curve combined by battery discharging and imported power in scenario 2. Therefore, the battery discharging curve in Fig. 14 represents the reduced grid imported power. Similarly, the exported power in scenario 1 can be represented by the curve combined by battery charging and exported power in scenario 2. Therefore, the battery charging curve in Fig. 14 represents the reduced grid exported power. It shows that part of the exported power and imported power in scenario 1 is directed to the battery charging and discharging processes in scenario 2 before the grid interaction, and thus, the grid interaction is reduced. Quantitatively, the battery effectively reduces the grid imported energy by 65.22% during this week. The grid-dependent time during the week is shortened from 55.57% of the time to 22.88% of the time.

5.3. The techno-economic analysis for the community energy system

This section will discuss and compare the techno-economic performance of the proposed community energy system. Table 8 summarises the key values selected for the techno-economic analysis. According to the RE cost database by IRENA [47], the global weighted average installed cost of offshore wind energy was 29,626 HKD/kW (3,800 USD/kW) in 2019. According to Chen [48], the construction cost of a tidal stream power plant at the US marine was about 19,101 HKD/kW (2,450 USD/kW) in 2013. Moreover, according to the cost and market potential report by the IRENA [49], the community-scale Li-ion battery cost was about 3,278 HKD/kWh (420 USD/kWh) in 2016. Furthermore, the interest rate adopted is a five-year average value recorded by the Worldbank from 2015 to 2019 [50]. In addition, the operation cycle of the community energy system is assumed to be 20 years. The community-scale battery is replaced every 8 years. Three FiT situations are considered in the analysis, namely, the RE generation based FiT scheme (FiT_1), export FiT scheme (FiT_2), and no FiT scheme. Table 9 summarises the calculation results of the economic performance.

For group 1 scenario 1, the economic performance of the community energy system decreases when the proportion of TSCs increases. Case 1 has the best economic benefit within the group – the NPV is 1,120.94 million HKD, and the DPP is 6.12 years with FiT_1. Therefore, although the hybrid RE system in case 5 successfully improves the system load matching, the electricity tariff saving gained by the additional reduction of grid interaction is insufficient to recover the additional investment costs as fast as case 1. In fact, the main reason for the inferior economic performance for cases with higher proportions of TSC is the low energy generation effectiveness and the low capacity factor of the Neptune NP1000, as mentioned in Section 3.3.2. In addition, it can be noticed that all of the 11 cases in group 1 are unprofitable with FiT_2 or without FiT in scenario 1. It indicates that the additional cost of system investment and operation cannot be recovered by the export FiT incentives and the electricity tariff saving within the 20-year operation cycle.

Table 8
Key parameters used for economic evaluation.

	CAPEX	O&M (% of CAPEX)	Ref.
OWT	29,626 HKD/kW (3,800 USD/kW)	5%	[47]
TSG	19,101 HKD/kW (2,450 USD/kW)	5%	[48]
Battery	3,278 HKD/kWh (420 USD/kWh)	reinvestment every 8 year	[49]
Interest rate	2.14%		[50]
FiT_1	3 HKD/kWh		[44]
CLP tariff / FiT_2	1.22 HKD/kWh		[45]

A similar trend can be observed in group 2 scenario 1 – case 1 has the best economic performance under FiT_1 and FiT_2, and the economic performance worsens as the proportion of TSC increases. However, under the situation without FiT, it is discovered that the system economic performance firstly increases as the proportion of TSC increases, and case 19 has the least bad economic performance among group 2. Such tend of the economic performance correlates with the annual OEM curve in Fig. 11**(b)**. Therefore, apart from the capital investment cost, OEM is another dominant factor that determines the system economic performance when FiT is unavailable, as it reflects the balance between the suitable system investment and the electricity tariff saving. Specifically, although case 1 achieves the target of net-zero and a higher OEF, 50.39% of the RE generation is exported to the grid without any benefit. While in case 19, 80.98% of the RE generation is consumed onsite, and the indirect economic loss caused by exporting the RE generation to the grid without any benefit is minimised. Therefore, when FiT is unavailable, the RE system in case 1 is considered largely oversized. As a result, although case 1 saves more electricity tariffs, it takes a longer time to recover the additional capital investment.

For group 1 scenario 2, the most profitable case is also case 1– the NPV is 447.36 million HKD, and the DPP is 11.74 years with the FiT_1. However, different from group 1 scenario 1, where cases with the higher proportion of TSCs are less profitable, case 5 has the second-best economic performance in group 1 scenario 2, and it is also the most profitable case among the 9 hybrid RE cases. Similar to group 1 scenario 1, all of the 11 cases are unprofitable with FiT_2 or without FiT in scenario 2. In addition, compared to group 1 scenario 1, a worse economic performance is observed for group 1 scenario 2, although the system load matching is significantly enhanced by the community-scale battery as indicated in Table 7 and Table 9.

To further investigate the techno-economic impacts of the battery, the performance of case 5 with a range of battery capacity from 0 to 70 MWh is calculated. The corresponding system load matching, the NPV, and the equivalent CO_2 emission are depicted in Fig. 15. It is found that the equivalent CO_2 emission will decrease with the increased battery capacity, which is a result of the reduced grid imported energy. In addition, the system economic performance also has a negative correlation against the technical performance under the situations with FiT_1 and without FiT. To be specific, when the battery capacity increases, the system load matching continuously improves while the NPV continuously decreases. Therefore, from the economic perspective, the optimal battery capacity is 0 MWh, indicating that the expensive investment and replacement costs of the battery will inevitably harm the economic performance, even if a larger battery capacity could further reduce the grid imported energy, and subsequently save more electricity tariff. With the determined battery capacities in Table 7, the battery cost should be substantially lowered so that the cases in group 1 scenario 2 can be considered as economically competitive as the cases in group 1 scenario 1. For example, the battery price for case 5 should be lowered to 644.27 HKD/kWh (82.64 USD/kWh), so that the same economic performance is achieved in scenario 1 and scenario 2. Furthermore, the NPV of case 5 scenario 2 under an assumed battery price of 389.82 HKD/kWh (50 USD/kWh) is plotted in Fig. 15. In this case, the optimal battery capacity with the highest NPV is determined at around 35 MWh. Therefore, when the battery price is low enough, there exists an optimal battery capacity that maximises the system economic performance. When the battery cost decreases further, the optimal battery capacity will shift towards a larger capacity.

To compare the market competitiveness of the different cases, Fig. 16 depicts the technical performance indicator OEF and the economic performance indicator NPV. It should be mentioned that, according to Eq. (8), the equivalent CO_2 emission is negatively correlated with OEF in a linear relationship. Specifically, when the OEF increases, the equivalent CO_2 emission decreases linearly. Therefore, OEF can be used to indirectly represent the equivalent CO_2 emission, and the higher value of OEF represents the lower equivalent CO_2 emission. Although the Pareto

Table 9
Summary of the system economic performance.

Group	Case	Scenario 1 (without batteries)				Scenario 2 (with batteries)			
		FiT_1		FiT_2	No FiT	FiT_1		FiT_2	No FiT
		NPV (Million HKD)	DPP (Years)	NPV (Million HKD)	NPV (Million HKD)	NPV (Million HKD)	DPP (Years)	NPV (Million HKD)	NPV (Million HKD)
Group 1 & 2	**1**	1,120.94	6.12	−152.80	−502.42	447.36	11.74	−935.84	−1,176.01
Group 1	**2**	998.45	7.20	−302.32	−630.19	80.60	18.90	−1,347.51	−1,548.04
	3	868.74	8.37	−445.60	−759.59	85.28	18.81	−1,356.52	−1,543.05
	4	733.64	9.69	−588.88	−894.39	101.92	18.53	−1,348.80	−1,526.10
	5	594.24	11.17	−732.16	−1,033.48	122.83	18.17	−1,332.69	−1,504.89
	6	450.48	12.88	−875.44	−1,176.93	113.62	18.24	−1,341.70	−1,513.79
	7	301.82	14.88	−1,018.72	−1,325.28	57.78	19.06	−1,392.67	−1,569.32
	8	147.22	17.29	−1,161.99	−1,479.58	−20.79	/	−1,460.40	−1,647.58
	9	−14.36	/	−1,305.27	−1,640.85	−124.31	/	−1,544.82	−1,750.80
	10	−183.41	/	−1,448.55	−1,809.59	−260.00	/	−1,654.50	−1,886.18
	11	−359.51	/	−1,591.83	−1,985.38	−412.12	/	−1,772.43	−2,037.99
Group 2	**12**	1,039.24	6.29	−165.05	−466.49				
	13	955.48	6.50	−177.29	−432.60				
	14	869.54	6.74	−189.53	−400.90				
	15	780.93	7.05	−201.78	−371.87				
	16	689.00	7.44	−214.02	−346.17				
	17	592.17	7.95	−226.26	−325.36				
	18	488.55	8.67	−238.51	−311.34				
	19	376.05	9.73	−250.75	−306.21				
	20	253.78	11.43	−262.99	−310.83				
	21	123.51	14.44	−275.24	−323.47				

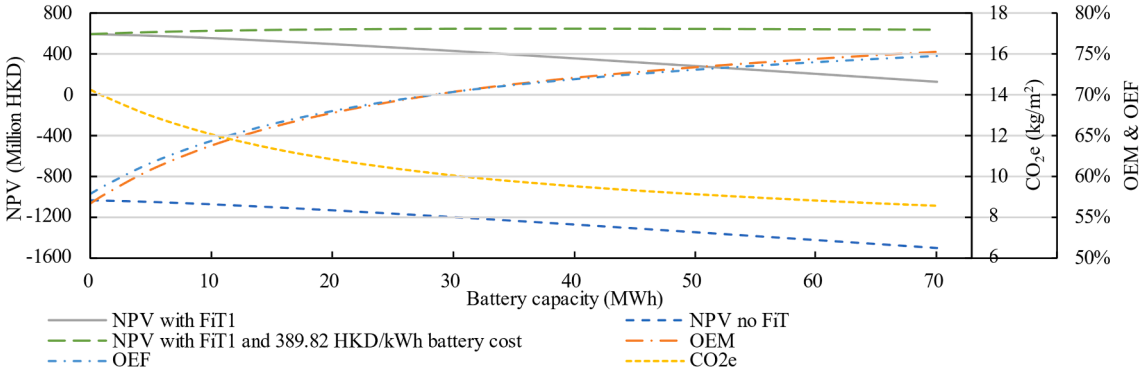

Fig. 15. Techno-economic performance of case 5 scenario 2 with varying battery capacity.

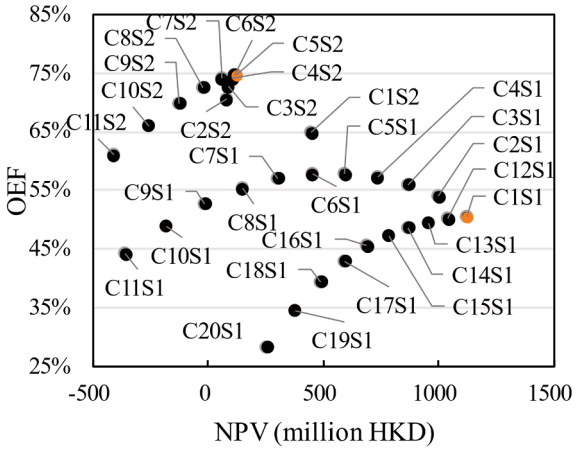

Fig. 16. Techno-economic comparison between group 1 scenario 1, group 1 scenario 2, and group 2 scenario 1.

front may not be visualized because of the limited simulation results, cases with a relatively balanced techno-economic performance can be determined, for example, case 5 scenario 2 and case 1 scenario 1. In summary, if one considers the technical performance as the priority for system selection, case 5 with battery could be the solution, as it achieves not only the almost best system load matching but also the best economic performance among the hybrid RE cases in scenario 2. However, in the situation where the economic performance is prioritized, case 1 without battery could be the suggested solution.

5.4. Sensitivity analysis

In this study, there is a large uncertainty associated with the costs chosen for the economic analysis, particularly the capital investment costs. Such uncertainties may affect the system economic performance significantly and may alter their economic superiority to each other. This section discusses the price uncertainty by calculating and comparing the system economic performance of group 1 under different capital investment price situations. Table 10 lists the 7 price situations considered in this sensitivity analysis. The price situation 1 has been

Table 10
Summary of the 6 price situations for sensitivity analysis.

	OWT (HKD/kW)	TSC (HKD/kW)
Price situation 1	29,626	19,101
Price situation 2	29,626	13,644 [48]
Price situation 3	29,626	30,796 [48]
Price situation 4	18,290 [51]	19,101
Price situation 5	18,290	13,644
Price situation 6	18,290	30,796
Price situation 7	Eq. (9)	Eq. (10)

calculated and analysed in 5.3. It should be mentioned that the 3 different capital installed prices of TSC are reported from three commercial tidal stream energy generation plants in the United States, specifically the Maine plant, nova Scotia plant, Massachusetts plant. They represent the middle, highest, and lowest installed costs reported in [48]. Fig. 17 summarises the sensitivity analysis results.

For price situations 1–6, case 1 and case 11 are the most profitable and the least profitable cases in scenario 1. The NPV falls almost linearly as the proportion of TSCs increases. The closest and furthest economic performance gap between case 1 and case 11 are observed under price situations 2 and 6. However, in scenario 2, the relative economic performance of each case to each other is much more sensitive to the change of capital investment cost. Under price situations 1–6, case 1 and case 11 are still the most profitable and the least profitable cases, except for price situation 2, where case 7 has the best economic performance because the TSC is much cheaper than the OWT. Therefore, one of the necessary conditions for cases with TSCs to economically outperform case 1 is that the capital installed cost for the TSC should be significantly lower than the OWT. The main reason is the higher system capacity required in these cases, and it is again the result of the low generation effectiveness and the low capacity factor of the TSC.

In addition to the different capital installed price levels, the scale of the system could be another factor that affects the system economic performance, as the unit capital installed cost can be significantly cut down by upscaling the system. For example, it is reported that the LCOE can be significantly cut down by 23% by upsizing the OWT and offshore wind farm [52]. A similar philosophy can be applied to the capital installed cost of TSC. According to [53], approximately 67% of the capital installed cost of an offshore wind farm is contributed by the OWTs, foundation, SCADA, cable, and the substation, while the rest of the costs are mainly induced from the installation and project management. Similarly, according to [54], approximately 80% of the capital investment cost of a tidal stream plant is contributed by the device, cable, foundation, and grid connection, while the rest of 20% is induced from the installation processes. To model the gradually decreasing capital installed cost as the system size increases, it is assumed that the capital installed costs induced from the installation and project management will gradually decrease as the system size increases. For OWT, it is assumed that 30% of the capital installed cost will reduce by 20% with each additional OWT. For TSC, it is assumed that 20% of the capital installed cost will reduce by 20% with each additional TSC. Therefore, the unit capital installed cost of OWT and TSC can be represented by Eq. (9) and Eq. (10), respectively.

$$CAPEX_{OWT} = 29,626 \times (0.7 + 0.3 \times 0.8^{n-1}) \tag{9}$$

$$CAPEX_{TSC} = 19,101 \times (0.8 + 0.2 \times 0.8^{n-1}) \tag{10}$$

where n represents the number of OWTs or TSCs.

The calculation results are plotted in Fig. 17. It is discovered that the curve representing price situation 7 remains the same pattern as with price situation 1. In other words, the gradually decreasing capital cost with the increasing system size is relatively insignificant to alter their economic superiority to each other. However, one significant impact of price situation 7 is that all 11 cases in scenario 1 and scenario 2 can achieve positive NPV after the 20-year operation cycle, and the NPVs increased noticeably when compared to price situation 1.

5.5. Additional options to achieve a coastal zero-energy community

In the proposed ZEC, it is assumed that approximately 10% of the rooftop area (1000 m^2) is deployed for solar thermal collectors. This section will discuss the possibility of further exploiting solar energy by an additional rooftop PV system, which covers approximately 70% of

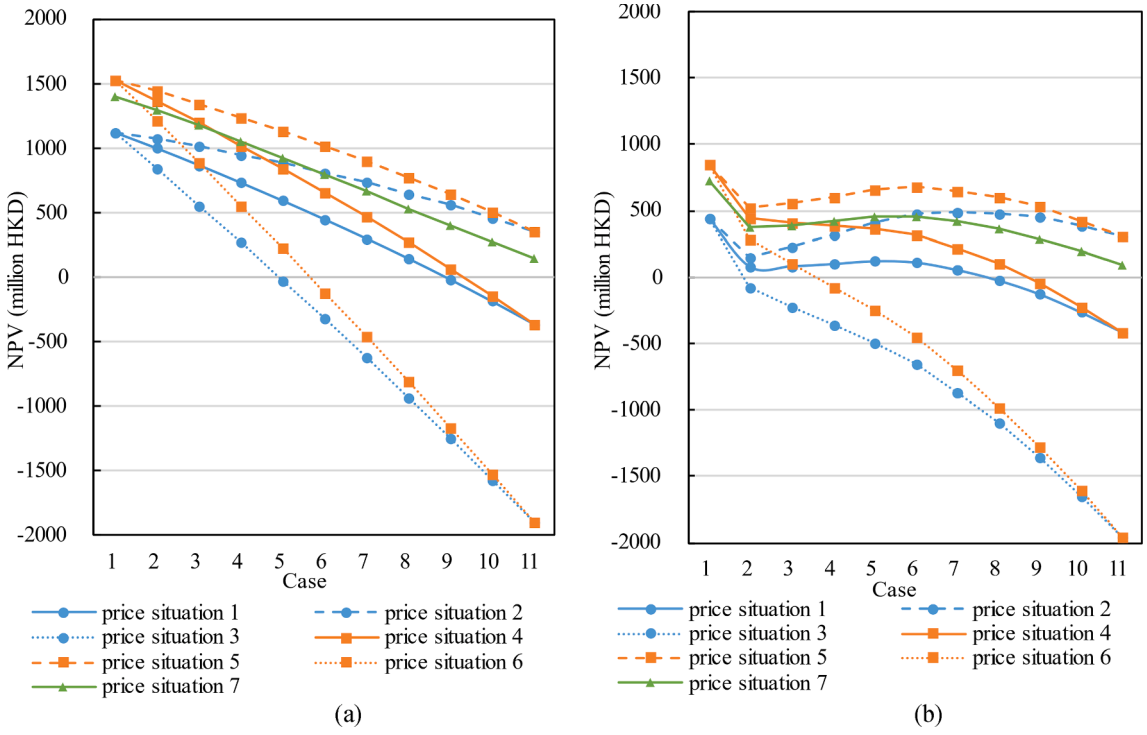

Fig. 17. Economic performance sensitivity analysis under FiT_1 (a) scenario 1; (b) scenario 2.

the community roof area (7000 m^2). The 20% roof area left is reserved for the installation of other building equipment. The default PV model Type 190c in the TRNSYS library is used. Each PV module has a rating capacity of 100 kWp under standard testing conditions. Specifically, the module voltage and current at the maximum power tracking point are 17 V and 5.9 A, respectively. In addition, the module area of each PV module is 0.89 m^2. Therefore, it is assumed that 7000 pieces of PV module will be installed, forming a 700 kW rooftop PV array. According to the RE cost database by IRENA [47], the global weighted average installed cost of solar photovoltaic energy was 7,867 HKD/kW (1,009 USD/kW) in 2019.

Table 11 lists the techno-economic performance of case 5 scenario 1, case 5 scenario 2, and case 5 scenario 1 with a rooftop PV system for comparison. The 700 kW PV array generated an additional 0.98 million kWh in a year, with an annual solar efficiency of 10.58%. Compared to case 5 scenario 1, the PV array caused a 0.1% decrease in the OEM and a 1.42% increase in OEF due to the additional RE generation. With the reduced grid imported energy, the annual equivalent CO_2 emission is subsequently reduced. When compared to case 5 scenario 2, the technical improvement achieved by the additional rooftop PV is insignificant due to the limited roof area and the limited PV capacity. However, the rooftop PV system improves the system economic performance noticeably, which is opposite to the negative economic impacts caused by the integration of the community-scale battery. Such an improvement of economic performance is largely due to the generation based FiT because the additional RE is credited with another stream of income that can recover the investment much faster the saving electricity tariff with the community-scale battery. Therefore, with the generation based FiT, it is best to customize the optimal mix of RE generation for the ZEC before the integration of the battery.

In addition to the additional rooftop PV system, a ZEC can also be achieved by connecting the community to a 100% RE super grid, which is a wide area electricity grid with distributed RE generation. By connecting to the super grid, the deployment of the offshore wind and tidal stream energy generation system can be less restricted by the proximity to the community. For example, in the context of the proposed coastal ZEC, locations with higher tidal stream velocities can be chosen for tidal stream energy generation. Such an option may significantly improve the techno-economic performance of cases with a relatively higher proportion of TSC because the major reason for their inferior techno-economic performance presented in this study is the low generation effectiveness and the low capacity factor of the Neptune NP1000. However, when connecting the community to a 100% RE super grid, the boundary of the ZEC should be clearly defined, as it inevitably involves grid services that may induce additional benefits and costs. Nonetheless, while the concept of a 100% RE super grid is futuristic, it is proven to be technically feasible and economically superior to other non-renewable alternatives such as nuclear energy and fossil carbon capture and storage in specific areas [55]. Furthermore, such a 100% RE super grid can significantly expand the scope of a ZEC from the currently studied 10-building coastal ZEC to a region-wide or even city-wide zero energy electricity grid, which is of great potential from the perspective of regional zero energy development.

Table 11
Comparison of case 5 scenario 1, case 5 scenario 2, and case 5 scenario 1 with a rooftop PV system.

	C5S1	C5S2	C5S1 + PV
System capacity (MW)	41.25	41.25	41.95
Annual generation (million kWh)	35.40	35.40	36.33
Annual OEM	56.68%	75.25%	56.58%
Annual OEF	57.84%	74.75%	59.26%
Equivalent CO_2 emission (kg/m^2)	14.27	8.55	13.79
NPV (million HKD)	594.24	122.83	636.93
DPP (years)	11.17	18.17	10.86

6. Conclusions

With the urgency in mitigating climate change, countries worldwide have been shifting towards a low-carbon economy by increasing the RE penetration. This study investigates the feasibility to reach a ZEC with the support of a hybrid offshore wind and tidal stream energy generation system, as well as an ocean and solar thermal energy supported district cooling and heating system. The dynamic system simulation tool TRNSYS is utilized to demonstrate a proposed ZEC with a typical community size – 8 high-rise residential buildings and 2 mid-rise office buildings with a 9.86 MW community peak power demand. The offshore wind energy and tidal stream energy are utilized for renewable energy generation, while the ocean and solar thermal energy supported district cooling and heating system is developed for energy conservation. Twenty-one renewable energy cases with the unique hybrid combination are formed and classified into 2 groups according to the annual generation and the system capacity. The system performance is investigated under 2 scenarios to discuss the dynamic impacts of grid interaction and electricity storage – scenario 1 without battery storage and scenario 2 with battery storage. The study assesses the system performance from the technical, economic, and emission perspectives by analysing the system load matching, NPV, DPP, and equivalent CO_2 emission. The techno-economic analysis evaluates the overall market competitiveness of the systems under three FiT schemes. The results in this paper could provide important insights into the developments of ZECs and hybrid offshore wind and tidal stream energy generation systems worldwide, especially for other densely populated coastal cities with significant energy demand. The important findings of the study are summarized below:

Firstly, the proposed ocean and solar thermal energy supported district cooling and heating system contributes to noticeable energy saving. By utilizing indirect seawater cooled chillers, a 6.61 annual AHU cooling system COP is reached, while a 7.05 annual space cooling system COP is reached. A higher cooling system efficiency is observed compared to the reference case, which utilizes the prevalent freshwater cooling towers. The main contributors are the more energy-efficient seawater cooled chiller and the less energy demanding seawater pumps. In addition, significant energy saving is observed in the district heating system, which achieves a 2.75 annual heating system COP. Compared to the reference case, which is fully supported by electric heaters, the proposed district heating system saves 71.40% of the annual heating energy consumption. Due to the significant heating energy saving, the average community EUI is lowered from 123.99 kWh/m^2 to 91.49 kWh/m^2. In addition, the community peak power is lowered by 19.58% from 12.26 MW to 9.86 MW.

Secondly, the optimal combination of the hybrid RE system and the integration of the community-scale battery can effectively improve the community system load matching, reduce the grid interaction, and lower the equivalent CO_2 emission. In group 1 scenario 1, case 5 with 6 OWTs (12 MW) and 117 TSCs (29.25 MW) has the best system load matching – the annual RE self-consumption index OEM is 56.68% and the annual load coverage index OEF is 57.84%. The ZEC is independent on the grid during 40.88% of the time in a year. The equivalent CO_2 emission is reduced from 45.88 kg/m^2 in the reference case to 14.27 kg/m^2. In scenario 2, the annual load matching index OEM and OEF of case 5 are raised to 75.25% and 74.75%, respectively. The battery effectively increases the grid-independent time to 64.59% of the time in a year. With the determined battery capacity, the equivalent CO_2 emission of case 5 is further reduced to 8.55 kg/m^2.

Thirdly, the techno-economic analysis reveals that, with the adopted price settings, offshore wind energy generation is more profitable than tidal stream energy generation for the coastal ZEC, and the community-scale battery diminishes system economic performance due to the current high battery price settings. In both scenario 1 and scenario 2, case 1 with only offshore wind energy generation has the best economic performance – the NPVs in scenario 1 and scenario 2 are 1,120.94 million

HKD and 447.36 million HKD, respectively. The system economic performance decreases continuously with the increasing proportion of TSCs, and the capital investment and operational cost of case 11 cannot be recovered within the 20-year operation cycle. Therefore, tidal stream energy generation by the Neptune NP 1000 is considered less competitive than offshore wind energy generation, mainly due to the low effectiveness in energy generation and low capacity factor. In addition, the comparison between scenario 1 and scenario 2 indicates that the community-scale Li-ion battery storage is less profitable due to its expensive investment cost and replacement cost. In case 5, in order to achieve superior economic performance than scenario 1, the battery price in scenario 2 should be significantly lowered from the current 3,278 HKD/kWh (420 USD/kWh) to less than 644.27 HKD/kWh (82.64 USD/kWh). In addition, when the battery price is lowe enough, there exists an optimal battery capacity that can further improve the system techno-economic performance.

Given the simulation and analysis settings, it was found that tidal stream energy generation is less competitive than offshore wind generation. The major obstacle is the low energy generation effectiveness and low capacity factor of the Neptune NP 1000 under low tidal speed environment. However, the situation could change in the future, as much research effort is being paid to the development of low-speed hydrokinetic turbines. When the technologies of the low-speed hydrokinetic turbines mature, the potential and market competitiveness of tidal stream energy generation ought to be reassessed. Furthermore, the major obstacle preventing the wider applications of offshore wind energy, tidal stream energy, and electricity storage remains the expensive investment cost. When the cost of these critical components drops in the future, the market competitiveness of the proposed community energy systems could be enhanced, especially for the cases with higher proportion of TSCs.

CRediT authorship contribution statement

Ming Li: Methodology, Investigation, Writing – original draft, Writing – review & editing. **Sunliang Cao:** Supervision, Funding acquisition, Project administration, Conceptualization, Methodology, Investigation, Writing – original draft, Writing – review & editing. **Xiaolin Zhu:** Methodology, Funding acquisition, Investigation, Writing – original draft, Writing – review & editing. **Yang Xu:** Methodology, Funding acquisition, Investigation, Writing – original draft, Writing – review & editing.

Declaration of Competing Interest

The authors declare that they have no known competing financial interests or personal relationships that could have appeared to influence the work reported in this paper.

Acknowledgement

This research is supported by the RISUD EFA funding, Project ID "P0033880" (Development of the frontier ocean energy technologies to utilize the renewable and storage resources of sea for supporting the seashore residential zero-energy communities) from Research Institute for Sustainable Urban Development (RISUD), The Hong Kong Polytechnic University. The third author also would like to acknowledge the support from the Hong Kong Polytechnic University (Project No. ZVN6) for partially supporting this research work.

References

[1] UNFCCC, 'The Paris Agreement'. https://unfccc.int/process-and-meetings/the-paris-agreement/the-paris-agreement.
[2] International Energy Agency, 'Global Energy Review 2021', 2021.
[3] International Renewable Energy Agency, 'Renewable energy statistics 2021', 2021.
[4] Carlisle N, Otto A, Geet V, Pless S. Definition of a "Zero Net Energy. Community' 2009.
[5] Gao P, Zheng J, Zhang J, Zhang T. Potential assessment of tidal stream energy around Hulu Island, China. Procedia Eng Jan. 2015;116(1):871–9. https://doi.org/10.1016/j.proeng.2015.08.376.
[6] Orhan K, Mayerle R. Assessment of the tidal stream power potential and impacts of tidal current turbines in the Strait of Larantuka, Indonesia. Energy Procedia Sep. 2017;125:230–9. https://doi.org/10.1016/j.egypro.2017.08.199.
[7] Marta-Almeida M, Cirano M, Soares CG, Lessa GC. A numerical tidal stream energy assessment study for Baía. Renew Energy 2017;107:271–87. https://doi.org/10.1016/j.renene.2017.01.047.
[8] Roberts A, et al. Current tidal power technologies and their suitability for applications in coastal and marine areas. J Ocean Eng Mar Energy 2016;2:227–45. https://doi.org/10.1007/s40722-016-0044-8.
[9] Lewis M, et al. A standardised tidal-stream power curve, optimised for the global resource. Renew Energy Jun. 2021;170:1308–23. https://doi.org/10.1016/J.RENENE.2021.02.032.
[10] Goss ZL, Coles DS, Kramer SC, Piggott MD. Efficient economic optimisation of large-scale tidal stream arrays. Appl Energy Aug. 2021;295:116975. https://doi.org/10.1016/J.APENERGY.2021.116975.
[11] Soudan B. Community-scale baseload generation from marine energy. Energy Dec. 2019;189:116134. https://doi.org/10.1016/j.energy.2019.116134.
[12] Pearre N, Adye K, Swan L. Proportioning wind, solar, and in-stream tidal electricity generating capacity to co-optimize multiple grid integration metrics. Appl Energy May 2019;242:69–77. https://doi.org/10.1016/J.APENERGY.2019.03.073.
[13] Lande-Sudall D, Stallard T, Stansby P. Co-located deployment of offshore wind turbines with tidal stream turbine arrays for improved cost of electricity generation. Renew Sustain Energy Rev Apr. 2019;104:492–503. https://doi.org/10.1016/j.rser.2019.01.035.
[14] Wen Y, Kamranzad B, Lin P. Assessment of long-term offshore wind energy potential in the south and southeast coasts of China based on a 55-year dataset. Energy Jun. 2021;224:120225. https://doi.org/10.1016/j.energy.2021.120225.
[15] Gao X, Yang H, Lin L, Koo P. Wind turbine layout optimization using multi-population genetic algorithm and a case study in Hong Kong offshore. J Wind Eng Ind Aerodyn Apr. 2015;139:89–99. https://doi.org/10.1016/j.jweia.2015.01.018.
[16] Caglayan DG, Ryberg DS, Heinrichs H, Linßen J, Stolten D, Robinius M. The techno-economic potential of offshore wind energy with optimized future turbine designs in Europe. Appl Energy Dec. 2019;255:113794. https://doi.org/10.1016/J.APENERGY.2019.113794.
[17] Schweizer J, et al. Investigating the potential and feasibility of an offshore wind farm in the Northern Adriatic Sea. Appl Energy Sep. 2016;177:449–63. https://doi.org/10.1016/j.apenergy.2016.05.114.
[18] Al-Nassar WK, Neelamani S, Al-Salem KA, Al-Dashti HA. Feasibility of offshore wind energy as an alternative source for the state of Kuwait. Energy Feb. 2019;169:783–96. https://doi.org/10.1016/j.energy.2018.11.140.
[19] Cali U, Erdogan N, Kucuksari S, Argin M. Techno-economic analysis of high potential offshore wind farm locations in Turkey. Energy Strateg Rev Nov. 2018;22:325–36. https://doi.org/10.1016/J.ESR.2018.10.007.
[20] Satir M, Murphy F, McDonnell K. Feasibility study of an offshore wind farm in the Aegean Sea, Turkey. Renew Sustain Energy Rev Jan. 2018;81:2552–62. https://doi.org/10.1016/j.rser.2017.06.063.
[21] Mattar C, Guzmán-Ibarra MC. A techno-economic assessment of offshore wind energy in Chile. Energy Aug. 2017;133:191–205. https://doi.org/10.1016/j.energy.2017.05.099.
[22] Maandal GLD, Tamayao-Kieke MAM, Danao LAM. Techno-Economic Assessment of Offshore Wind Energy in the Philippines. J Mar Sci Eng Jul. 2021;9(7):758. https://doi.org/10.3390/JMSE9070758.
[23] Nagababu G, Kachhwaha SS, Savsani V. Estimation of technical and economic potential of offshore wind along the coast of India. Energy Nov. 2017;138:79–91. https://doi.org/10.1016/J.ENERGY.2017.07.032.
[24] Liu X, Li N, Mu H, Li M, Liu X. Techno-energy-economic assessment of a high capacity offshore wind-pumped-storage hybrid power system for regional power system. J Energy Storage Sep. 2021;41:102892. https://doi.org/10.1016/J.EST.2021.102892.
[25] Li B, DeCarolis JF. A techno-economic assessment of offshore wind coupled to offshore compressed air energy storage. Appl Energy Oct. 2015;155:315–22. https://doi.org/10.1016/J.APENERGY.2015.05.111.
[26] Simpson JG, Hanrahan G, Loth E, Koenig GM, Sadoway DR. Liquid metal battery storage in an offshore wind turbine: Concept and economic analysis. Renew Sustain Energy Rev Oct. 2021;149:111387. https://doi.org/10.1016/J.RSER.2021.111387.
[27] Fouad MM, Iskander J, Shihata LA. Energy, carbon and cost analysis for an innovative zero energy community design. Sol Energy Aug. 2020;206:245–55. https://doi.org/10.1016/j.solener.2020.05.048.
[28] Lopes RA, Martins J, Aelenei D, Lima CP. A cooperative net zero energy community to improve load matching. Renew Energy Aug. 2016;93:1–13. https://doi.org/10.1016/j.renene.2016.02.044.
[29] Barone G, Buonomano A, Forzano C, Giuzio GF, Palombo A. Increasing renewable energy penetration and energy independence of island communities: A novel dynamic simulation approach for energy, economic, and environmental analysis, and optimization. J Clean Prod Aug. 2021;311:127558. https://doi.org/10.1016/J.JCLEPRO.2021.127558.
[30] Jahangir MH, Shahsavari A, Vaziri Rad MA. Feasibility study of a zero emission PV/Wind turbine/Wave energy converter hybrid system for stand-alone power supply: A case study. J Clean Prod Jul. 2020;262:121250. https://doi.org/10.1016/J.JCLEPRO.2020.121250.

[31] Vindel E, Berges M, Akinci B. Energy sharing through shared storage in net zero energy communities. *J Phys Conf Ser*, Nov 2019;1343(1):12107. https://doi.org/10.1088/1742-6596/1343/1/012107.
[32] Liu J, Chen X, Yang H, Shan K. Hybrid renewable energy applications in zero-energy buildings and communities integrating battery and hydrogen vehicle storage. Appl Energy May 2021;290:116733. https://doi.org/10.1016/J.APENERGY.2021.116733.
[33] He Y, Zhou Y, Yuan J, Liu Z, Wang Z, Zhang G. Transformation towards a carbon-neutral residential community with hydrogen economy and advanced energy management strategies. Energy Convers Manage Dec. 2021;249:114834. https://doi.org/10.1016/J.ENCONMAN.2021.114834.
[34] Garcia Novo P, Kyozuka Y. Tidal stream energy as a potential continuous power producer: A case study for West Japan. Energy Convers Manage 2021;245:114533. https://doi.org/10.1016/J.ENCONMAN.2021.114533.
[35] 'TRNSYS : Transient System Simulation Tool'. http://www.trnsys.com/index.html#1.
[36] Hong Kong Housing Authority and Housing Department, 'Standard Block Typical Floor Plans '. https://www.housingauthority.gov.hk/en/global-elements/estate-locator/standard-block-typical-floor-plans/.
[37] Hong Kong Government, 'Hong Kong Tidal Stream Prediction Service'. https://www.gov.hk/en/residents/transport/vessel/tidal_stream.htm.
[38] Ye Y, Shi Y, Cai N, Lee J, He X. Electro-thermal modeling and experimental validation for lithium ion battery. J Power Sources Feb. 2012;199:227–38. https://doi.org/10.1016/J.JPOWSOUR.2011.10.027.
[39] Sanaye S, Hajabdollahi H. Thermal-economic multi-objective optimization of plate fin heat exchanger using genetic algorithm. Appl Energy Jun. 2010;87(6):1893–902. https://doi.org/10.1016/J.APENERGY.2009.11.016.
[40] Hitachi, 'Performance : Wind Turbine'. https://www.hitachi.com/products/energy/wind/products/htw2000_80/performance/index.html.
[41] Hardisty J. The Tidal Stream Power Curve: A Case Study. Energy Power Eng 2012;04(03):132–6. https://doi.org/10.4236/epe.2012.43018.
[42] Dong Y, et al. Development of a 300 kW horizontal-axis tidal stream energy conversion system with adaptive variable-pitch turbine and direct-drive PMSG. Energy Jul. 2021;226:120361. https://doi.org/10.1016/J.ENERGY.2021.120361.
[43] Cao S, Hasan A, Sirén K. On-site energy matching indices for buildings with energy conversion, storage and hybrid grid connections. Energy Build Sep. 2013;64:423–38. https://doi.org/10.1016/j.enbuild.2013.05.030.
[44] 'GovHK: Feed-in Tariff'. https://www.gov.hk/en/residents/environment/renewable/feedintariff.htm.
[45] CLP, 'CLP Power Freezes 2021 Tariff and Introduces Over HK$160 Million Worth of Community Support Programmes', 2020.
[46] CLP, 'Sustainability Report 2020'. https://sustainability.clpgroup.com/en/2020/.
[47] International Renewable Energy Agency, 'Global weighted average total installed costs, capacity factors and LCOE 2010-2019'. https://www.irena.org/Statistics/View-Data-by-Topic/Costs/Global-Trends.
[48] Chen F. The Kuroshio Power Plant. Lect Notes Energy 2013;15. https://doi.org/10.1007/978-3-319-00822-6.
[49] International Renewable Energy Agency, 'Electricity storage and renewables: Costs and markets to 2030'. https://www.irena.org/publications/2017/oct/electricity-storage-and-renewables-costs-and-markets.
[50] The World Bank, 'Real interest rate (%) - Hong Kong SAR, China'. https://data.worldbank.org/indicator/FR.INR.RINR?end=2019&locations=HK&start=2010&view=chart.
[51] National Renewable EnergyLaboratory, 'No Title'. https://www.nrel.gov/index.html.
[52] Department of Energy, 'The Future of Offshore Wind Is Big—Literally'. https://www.energy.gov/eere/wind/articles/future-offshore-wind-big-literally.
[53] Blanco MI. The economics of wind energy. Renew Sustain Energy Rev Aug. 2009;13(6–7):1372–82. https://doi.org/10.1016/J.RSER.2008.09.004.
[54] Vazquez A, Iglesias G. Capital costs in tidal stream energy projects – A spatial approach. Energy Jul. 2016;107:215–26. https://doi.org/10.1016/J.ENERGY.2016.03.123.
[55] Bogdanov D, Breyer C. North-East Asian Super Grid for 100% renewable energy supply: Optimal mix of energy technologies for electricity, gas and heat supply options. Energy Convers Manage Mar. 2016;112:176–90. https://doi.org/10.1016/J.ENCONMAN.2016.01.019.